

# Machine Learning Coarse-Grained Potentials of Protein Thermodynamics

Maciej Majewski,<sup>†,‡,§§</sup> Adrià Pérez,<sup>†,‡,§§</sup> Philipp Thölke,<sup>†</sup> Stefan Doerr,<sup>‡</sup>  
 Nicholas E. Charron,<sup>¶,§,||</sup> Toni Giorgino,<sup>⊥</sup> Brooke E. Husic,<sup>#, @, △, ▽</sup> Cecilia  
 Clementi,<sup>\*, ||, §, ¶, ††</sup> Frank Noé,<sup>\*, #, ||, ††, ‡‡</sup> and Gianni De Fabritiis<sup>\*, †, ‡, ¶, ¶</sup>

<sup>†</sup>*Computational Science Laboratory, Universitat Pompeu Fabra, Barcelona Biomedical Research Park (PRBB), Carrer Dr. Aiguader 88, 08003, Barcelona, Spain*

<sup>‡</sup>*Acellera Labs, Doctor Trueta 183, 08005, Barcelona, Spain*

<sup>¶</sup>*Department of Physics, Rice University, Houston, TX 77005, USA*

<sup>§</sup>*Center for Theoretical Biological Physics, Rice University, Houston, TX 77005, USA*

<sup>||</sup>*Department of Physics, FU Berlin, Arnimallee 12, 14195 Berlin, Germany*

<sup>⊥</sup>*Biophysics Institute, National Research Council (CNR-IBF), 20133 Milan, Italy*

<sup>#</sup>*Department of Mathematics and Computer Science, FU Berlin, Arnimallee 12, 14195 Berlin, Germany*

<sup>@</sup>*Lewis Sigler Institute for Integrative Genomics, Princeton University, Princeton, NJ 08540, United States*

<sup>△</sup>*Princeton Center for Theoretical Science, Princeton University, Princeton, NJ 08540, United States*

<sup>▽</sup>*Center for the Physics of Biological Function, Princeton University, Princeton, NJ 08540, United States*

<sup>††</sup>*Department of Chemistry, Rice University, Houston, TX 77005, USA*

<sup>‡‡</sup>*Microsoft Research Cambridge, United Kingdom*

<sup>¶¶</sup>*Institució Catalana de Recerca i Estudis Avançats (ICREA), Passeig Lluís Companys 23, 08010 Barcelona, Spain*

<sup>§§</sup>*Equal contribution*

E-mail: [cecilia.clementi@fu-berlin.de](mailto:cecilia.clementi@fu-berlin.de); [frank.noe@fu-berlin.de](mailto:frank.noe@fu-berlin.de); [gianni.defabritiis@upf.edu](mailto:gianni.defabritiis@upf.edu)

## Abstract

A generalized understanding of protein dynamics is an unsolved scientific problem, the solution of which is critical to the interpretation of the structure-function relationships that govern essential biological processes. Here, we approach this problem by constructing coarse-grained molecular potentials based on artificial neural networks and grounded in statistical mechanics. For training, we build a unique dataset of unbiased all-atom molecular dynamics simulations of approximately 9 ms for twelve different proteins with multiple secondary structure arrangements. The

coarse-grained models are capable of accelerating the dynamics by more than three orders of magnitude while preserving the thermodynamics of the systems. Coarse-grained simulations identify relevant structural states in the ensemble with comparable energetics to the all-atom systems. Furthermore, we show that a single coarse-grained potential can integrate all twelve proteins and can capture experimental structural features of mutated proteins. These results indicate that machine learning coarse-grained potentials could provide a feasible approach to simulate and understand protein dynamics.

## Introduction

Proteins are complex dynamical systems that exist in an equilibrium of distinct conformational states, and their multi-state behavior is critical for their biological functions.<sup>1-5</sup> A complete description of the dynamics of a protein requires the determination of (1) its stable and metastable conformational states, (2) the relative probabilities of these states and (3) the rates of interconversion among them. Here, we focus on addressing the first two problems by demonstrating how to learn coarse-grained potentials that preserve protein thermodynamics.

Due to the structural heterogeneity of proteins and the ranges of time and length scales over which their dynamics occur, there is no single technique that is able to successfully model protein behavior across the whole spatiotemporal scale. Computationally, the main method to study protein dynamics has traditionally been molecular dynamics (MD). The first MD simulation ever made was carried out in 1977 on the BPTI protein in vacuum, and only accounted for 9.2 picoseconds of simulation time.<sup>6</sup> As remarked by Karplus & McCammon,<sup>7</sup> these simulations were pivotal towards the realization that proteins are dynamic systems and that those dynamics play a fundamental role in their biological function.<sup>2</sup> When compared with experimental methods such as X-ray crystallography, MD simulations may obtain a complete description of the *dynamics* in atomic resolution. This information can explain slow events at the millisecond or microsecond timescale, typically with a femtosecond time resolution.

In the last several decades, there have been many attempts to better understand protein dynamics by long unbiased MD. For example, Lindorff-Larsen *et al.*<sup>8</sup> and Piana *et al.*<sup>9</sup> simulated several proteins that undergo multiple folding events over the course of micro- to millisecond trajectories, yielding crucial insights into the hierarchy and timescales of the various structural rearrangements. With current technological limitations, unbiased MD is not capable of describing longer-timescale events, such as the dynamics of large proteins or the formation of multi-protein complexes. Due to the computational cost and timescales involved, there are just a few exam-

ples of modelling of such events, including folding of a dimeric protein Top7-CFr<sup>10</sup> and all-atom computational reconstruction of protein-protein (Barnase-Barstar) recognition.<sup>11</sup> Many methods have been developed to alleviate these sampling limitations, for instance, umbrella sampling,<sup>12</sup> biased Monte Carlo methods<sup>13</sup> and biased molecular dynamics like replica-exchange,<sup>14,15</sup> steered MD<sup>16,17</sup> and metadynamics.<sup>18</sup> More recently, a new generative method based on normalizing flows has been proposed to sample structures from the Boltzmann distribution in “one-shot”, thereby avoiding the many steps needed in MD to sample different metastable states.<sup>19,20</sup>

Another way to access the timescales of slow biological processes is through the use of coarse-graining (CG) approaches. Coarse-graining has a long history in the modelling of protein dynamics<sup>21,22</sup> and since the pioneering work of Levitt and Warshel,<sup>23</sup> many different approaches to CG have been proposed.<sup>24-29</sup> Popular CG approaches include structure-based models,<sup>30</sup> MARTINI,<sup>31,32</sup> CABS,<sup>33</sup> AWSEM,<sup>34</sup> and Rosetta.<sup>35</sup> In general, a CG model consists of two parts: the selection of the CG resolution (or mapping) and the design of an effective energy function for the model once the mapping has been assigned. Although recent work has attempted to combine these two points,<sup>36</sup> they are in general kept distinct. The choice of an “optimal” mapping strategy is still an open research problem<sup>37,38,39</sup> and we will assume in the following that the mapping is given, focusing instead on the second point, which is the choice of an energy function for the CG model that can reproduce relevant properties of the fine-grained system. Recently, our groups and others have used machine learning methods to extend the theoretical ideas of coarse-graining to systems of practical interest, which provides a systematic and general solution to reduce the degrees of freedom of a molecular system by building a potential of mean force over the coarse-grained system.<sup>40-46</sup>

Machine learning models, in particular neural network potentials (NNPs), can learn fast, yet accurate, potential energy functions for use in MD simulations by training on large-scale databases obtained from more expensive approaches.<sup>42,43,47-50</sup> One particularly interesting feature of machine learning potentials is that they

Table 1: All-atom MD simulation dataset generated for this work and used for training and testing of NNPs.

Protein	Sequence length (#aa)	Aggregated time ( $\mu$ s)	Min. RMSD ( $\text{\AA}$ )
Chignolin	10	186	0.15
Trp-Cage	20	195	0.45
BBA	28	362	1.13
WW-Domain	34	1362	0.73
Villin	35	234	0.47
NTL9	39	776	0.32
BBL	47	677	1.55
Protein B	47	608	1.19
Homeodomain	54	198	0.56
Protein G	56	2266	0.55
$\alpha$ 3D	73	768	1.81
$\lambda$ -repressor	80	1422	0.82

can learn many-body atomic interactions.<sup>51</sup> A steady level of improvement of the methodology over the years has led to dozens of novel and better modelling architectures for predicting the energy of small molecules. The first important contributions are rooted in the seminal works by Behler and Parrinello<sup>52</sup> and Rupp et al.<sup>53</sup>. One of the earliest transferable machine learning potentials for biomolecules, ANI-1,<sup>54</sup> is based on Behler-Parrinello (BP) representation, while other models use more modern graph convolutions.<sup>55–57</sup>

In this work, we investigate twelve non-trivial protein systems with a variety of secondary structural elements. We build a unique multi-millisecond dataset of unbiased all-atom MD simulations of studied proteins. We show the recovery of experimental conformations starting from disordered configurations through the classical Langevin simulations of a machine-learned CG force field. We demonstrate that generalization across macromolecular systems is possible by using a multi-protein machine learning potential for all the targets. Finally, we investigate the predictive capabilities of the NNP through simulation and analysis of selected mutants (i.e., sequences outside of the training set).

## Results and Discussion

**Multi-millisecond all-atom molecular dynamics dataset.** We created a large-scale dataset of

all-atom MD simulations by selecting twelve fast-folding proteins, studied previously by Kubelka *et al.*<sup>58</sup> and Lindorff-Larsen *et al.*<sup>8</sup> These proteins contain a variety of secondary structural elements, including  $\alpha$ -helices and  $\beta$ -strands, as well as unique tertiary structures and various lengths from 10 to 80 amino acids. In the case of the shortest proteins, Chignolin and Trp-Cage (up to 20 amino acids), the secondary structure is quite simple. In general, the dataset contains a higher proportion of  $\alpha$ -helical proteins. The exceptions are the  $\beta$ -turn present in Chignolin, the mostly  $\beta$ -sheet structure of WW-Domain, and the mixed  $\alpha\beta$  structures of BBA, NTL9 and Protein G (Fig. 1). The dataset was generated by performing MD on each of the proteins starting from random coil conformations, simulating their whole dynamics and reaching the native structure. The total size of the dataset amounts to approximately 9 ms of simulation time across all proteins (Table 1). The dataset is available for download as a part of Supporting Information.

**Coarse-grained neural network potentials.** A common approach to bottom-up coarse-graining is to seek thermodynamic consistency; i.e. the equilibrium distribution sampled by the CG model—and thus all thermodynamic quantities computable from it, such as folding free energies—should match those of the all-atom model. Popular approaches to train thermodynamically consistent CG models are relative entropy minimization<sup>59</sup> and variational force matching.<sup>27,60</sup> The latter has recently been developed into a machine-learning approach to train NNPs to compute the CG energy.<sup>42,43</sup>

Let  $\mathbb{D}$  be a dataset of  $M$  coordinate-force pairs obtained using an all-atom MD force field. Conformations are given by  $\mathbf{r}_c \in \mathbb{R}^{3N_c}$ ,  $c = 1, \dots, M$  and forces by  $\mathbf{F}(\mathbf{r}_c) \in \mathbb{R}^{3N_c}$ , where  $N_c$  is the number of atoms in the system. The number of atoms  $N_c$  depends on  $c$  as we wish to also have different protein systems in the dataset  $\mathbb{D}$ . We define a linear mapping  $\Xi$  which reduces the dimensionality of the atomistic system  $\mathbf{x} = \Xi\mathbf{r} \in \mathbb{R}^{3n}$ , where  $n$  are the remaining degrees of freedom. For example,  $\Xi$  could be a simple map to  $\alpha$ -carbon atom coordinates for each amino acid, to backbone coordinates or to the center of mass. We seek to obtain  $U(\mathbf{x}_c; \boldsymbol{\theta}) : \mathbb{R}^{3n} \rightarrow \mathbb{R}$  for any configuration  $c$

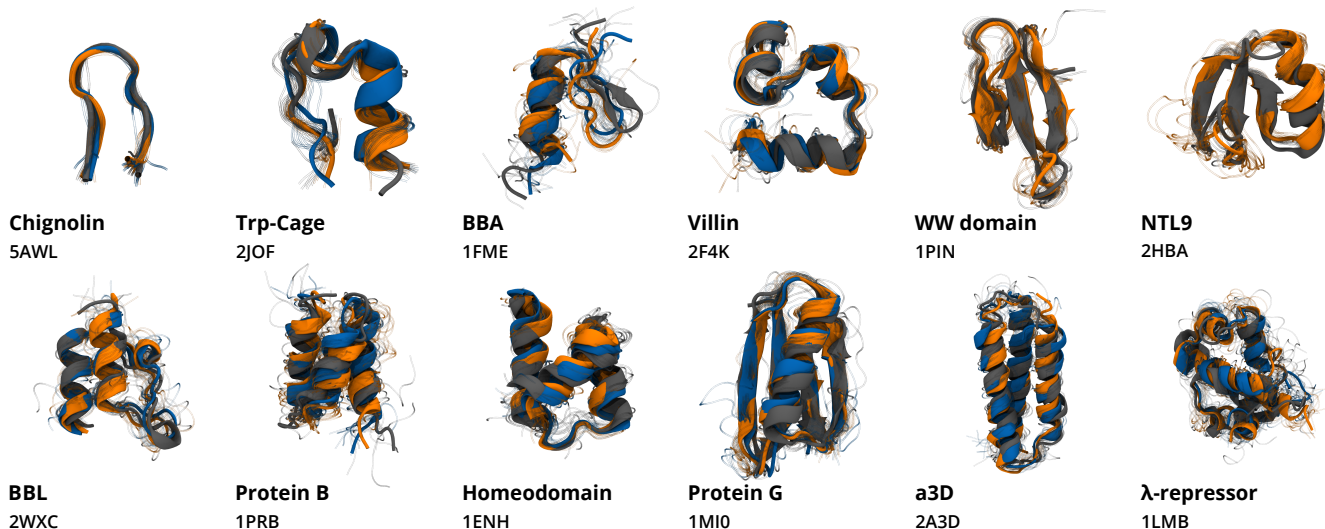


Figure 1: Structures obtained from CG simulations of the protein-specific model (orange) and the general multi-protein-trained model (blue), compared to their respective experimental structures (grey). Structures were sampled from the native macrostate, which was identified as the macrostate containing the conformation with the minimum RMSD with respect to the experimental crystal structure. Ten conformations were sampled from each conformational state (visualized as transparent shadows) and the lowest RMSD conformation of each macrostate is displayed in cartoon representation, reconstructing the backbone structure from  $\alpha$ -carbon atoms. The native conformation of each protein, extracted from their corresponding crystal structure is shown in opaque grey. The text indicates the protein name and PDB ID for the experimental structure. WW-Domain and NTL9 results for the general model are not shown, as the model failed to recover the experimental structures. The statistics of native macrostates are included in Table 2.

parameterized in  $\theta$ , such that to minimize the loss

$$L(\mathbf{R}; \theta) = \frac{1}{3nM} \sum_{c=1}^M \|\Xi \mathbf{F}(\mathbf{r}_c) + \nabla U(\Xi \mathbf{r}_c; \theta)\|^2 \quad (1)$$

In order to reduce the conformational space accessible during the CG simulation and prevent the system from poor exploration, it is important to provide a prior potential.<sup>43,61</sup> This also serves to reduce the complexity of the force field learning problem, and can equivalently be viewed as imposing physical biases from domain knowledge. The NNP is therefore performing a delta-learning between the all-atom forces and the prior forces. We applied bonded and repulsive terms to avoid rupture of the protein chain as well as clashing beads (Equations 11 and 12 in Supporting Information). Furthermore, we enforce chirality by introducing a dihedral prior term (Equation 13 in Supporting Information). This prevents the CG proteins from exploring mirror images of the na-

tive structures. The functional forms and parameters of all prior terms are available in the Supporting Information.

CG representations were created by retaining only certain atoms of each protein’s all-atom representation; the retained atoms are referred to as CG “beads”. NNPs were trained to predict forces based on the coordinates and identities of the beads, where the latter is represented as an embedding vector. Each CG bead comprises the  $\alpha$ -carbon atom of its amino acid, and each amino acid was described by a unique bead type. In previous work, we experimented with both  $\alpha$ -carbon and  $\alpha\beta$ -carbon representation; however, the simpler  $\alpha$ -carbon representation was sufficient to learn the dynamics of small proteins.<sup>62</sup>

**Coarse-grained molecular dynamics with neural network potentials reconstructs the dynamics of proteins.** Initially, we carried out CG simulations of all twelve proteins using the models trained on individual all-atom MD datasets corresponding to each protein; that is, we trained twelve



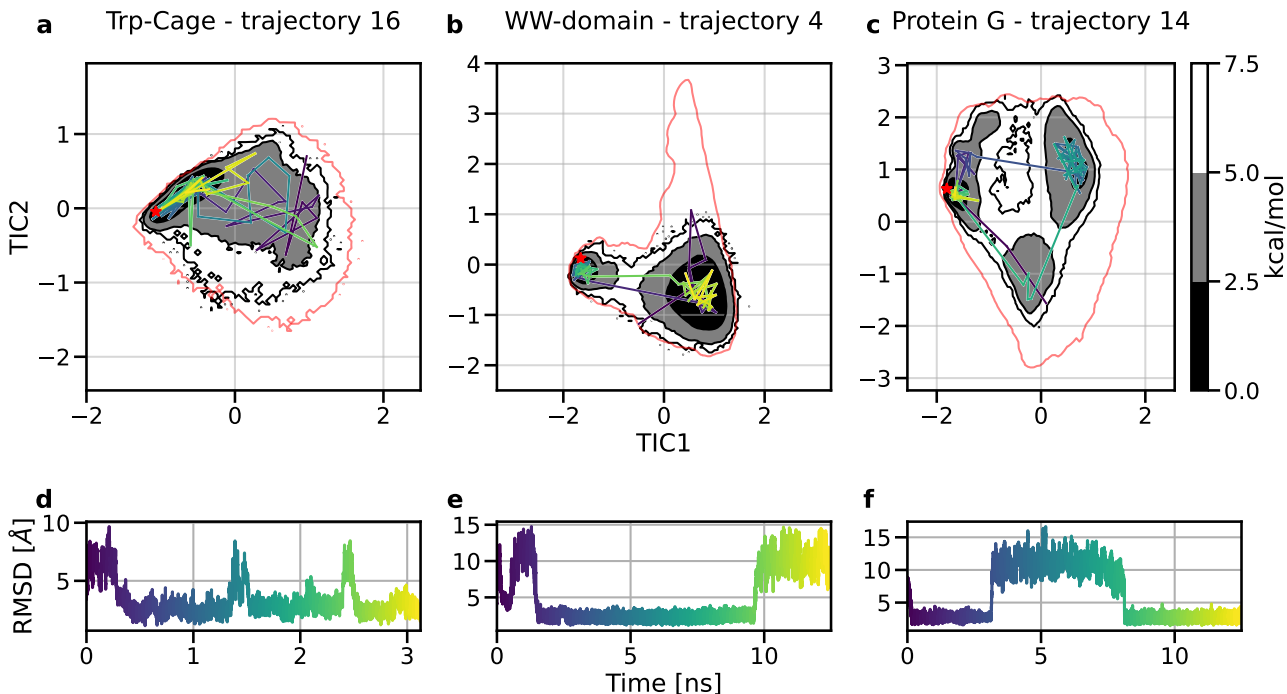


Figure 2: Three individual CG trajectories selected from validation MD of Trp-Cage, WW-Domain and Protein G. Each visualized simulation, coloured from purple to yellow, explores the free energy surface, accesses multiple major basins and transitions among conformations. Top panels: 100 states sampled uniformly from the trajectory plotted over CG free energy surface, projected over the first two time-lagged independent components (TICs) for Trp-Cage (a), WW-Domain (b) and Protein G (c). The red line indicates the all-atom equilibrium density by showing the energy level above the free energy minimum with the value of 7.5 kcal/mol. The experimental structure is marked as a red star. Bottom panels:  $C\alpha$ -RMSD of the trajectory with reference to the experimental structure for Trp-Cage (d), WW-Domain (e) and Protein G (f).

models, each one only using the corresponding data for one protein. To validate the models, we performed 32 parallel coarse-grained simulations for each target, starting from conformations sampled across the reference free energy surface, built based on all-atom MD (Supporting Fig. 1). The intent was to explore the conformational dynamics, sample the native structure and reconstruct the reference free energy surface.

A Markov state model (MSM)<sup>63–67</sup> analysis of CG simulations shows that all of the individual protein models were able to recover the experimental structure of the corresponding target (Fig. 1), accurately predicting all the secondary structure elements and the tertiary structure, with loops and unstructured terminal regions being the most variable parts. For the simplest target, Chignolin, the average root-mean-square deviation (RMSD)

value of the native macrostate was 0.7 Å. For less trivial structures, such as WW-Domain or NTL9, the values were below 2.5 Å. For even more complex arrangements of secondary elements, like Protein B and  $\lambda$ -repressor, the average RMSD of the native macrostate predicted by the network increased to 5.5 and 4.2 Å, respectively. In all cases, however, the network was able to sample conformations below 2.5 Å and global distance test (GDT)<sup>68</sup> scores above 60 (Table 2).

For all protein-specific models, simulations were able to sample folding events, in which the protein goes from a random coil to a native conformation (Fig. 2). The dynamics of transitions is accelerated more than three orders of magnitude, as the process happens in nanosecond timescale, in contrast to microseconds in the case of all-atom MD.<sup>8</sup> Additionally, individual trajectories were able to

explore the conformational landscape and transition between different metastable states observed in the original all-atom trajectories. For each protein, a representative trajectory is shown in a video included in Supporting Information (Supporting Table 3). A few models, in particular Homeodomain,  $\alpha$ 3D and  $\lambda$ -repressor, failed to sample direct transitions from ordered to disordered conformations (Supporting Fig. 5). This could have been caused partially by the model over-stabilizing the native structure.

**Coarse-grained potentials maintain the energetic landscape.** In order to estimate the equilibrium distribution and approximate the free energy surfaces from the CG simulations, we built MSMs for each CG simulation set. Time-lagged independent component analysis (TICA)<sup>69,70</sup> was used to project coarse-grained trajectories onto the first three components, using covariances computed from reference all-atom MD. Overall, the MSMs were able to recover the surface describing the dynamics, correctly locating the position of the global minimum in the free energy surface for all cases except Protein B (Supporting Fig. 2 and 4). The most ill-defined regions of TIC space correspond to unstructured conformations, which are more difficult for the models to sample. In most of the models, simulations transition rapidly to the native structure, and only the surface around the global minimum is sampled. This is particularly true for larger helical proteins, such as Homeodomain,  $\alpha$ 3D and  $\lambda$ -repressor, where the space explored falls mostly around the native structure. Alternatively, in Chignolin, Trp-Cage, Villin, NTL9 and Protein G, the models are able to sample most of the free energy surface, locating all different metastable minima identified through TICA.

In the case of Protein G, the model was able to identify all the metastable states, sharing similar features as the reference all-atom MD simulations (Fig. 3). Furthermore, the model correctly replicates the main transition to the native structure and allows for a possible interpretation of the folding pathway. In the most probable folding pathway, the protein initially forms an intermediate, partially folded state containing the  $\alpha$ -helix and the first hairpin. Next, the native structure is completed by the formation of the second hairpin. Al-

ternatively, a second pathway is possible where the structure goes through a misfolded state with an almost complete native structure except for the first hairpin, which shows increased flexibility. This replicates the results of all-atomistic MD simulations performed by Lindorff-Larsen *et al.*<sup>8</sup> The variant simulated both there and in this study is intermediate in sequence between the wild type and redesigned NuG2 variant. Despite high similarities in the sequence, experiments show that these variants exhibit distinct folding pathways. The difference is in the order of formation of the elements of  $\beta$ -sheet; in the wild-type variant of Protein G, the second hairpin folds before the first hairpin<sup>71,72</sup> while in the NuG2 variant the order is reversed.<sup>73</sup> The CG simulation using NNP shows the majority of flow going into the NuG2 variant folding, which agrees with one of the possible folding pathways. Additionally, the simulation correctly recovered the minima around the native conformation of Protein G, however, the position of the other minima on the free energy surface are less similar. In general, the force-matching method does not preserve kinetics,<sup>27,60</sup> so the height of the energy barriers is not expected to be accurately captured, as shown in the free energy plot (Supporting Fig. 4).

**A general multi-protein-trained model recovers the native structures of most reference proteins.** The individual CG models recovered native structures of the proteins, demonstrating the success of our approach for complex structures. These NNPs are, however, limited to the individual targets they were trained on. In the next step, we examined if it was possible to train a single, general model using the reference simulation data of all the protein targets (Supporting Fig. 6). We then simulated all targets with the general model, in the same way we did for the protein-specific models. The main objective of the general model is to match the results of individual models using a single CG potential.

The CG simulations show that the general model is able to reproduce the native structure of most of the proteins, with the exception of NTL9 and WW-Domain (Fig. 1 and Supporting Fig. 4). We identify each native macrostate based on its RMSD to the corresponding experimental structure. However, a simple criterion of minimal potential energy produced by the NNP is able to correctly

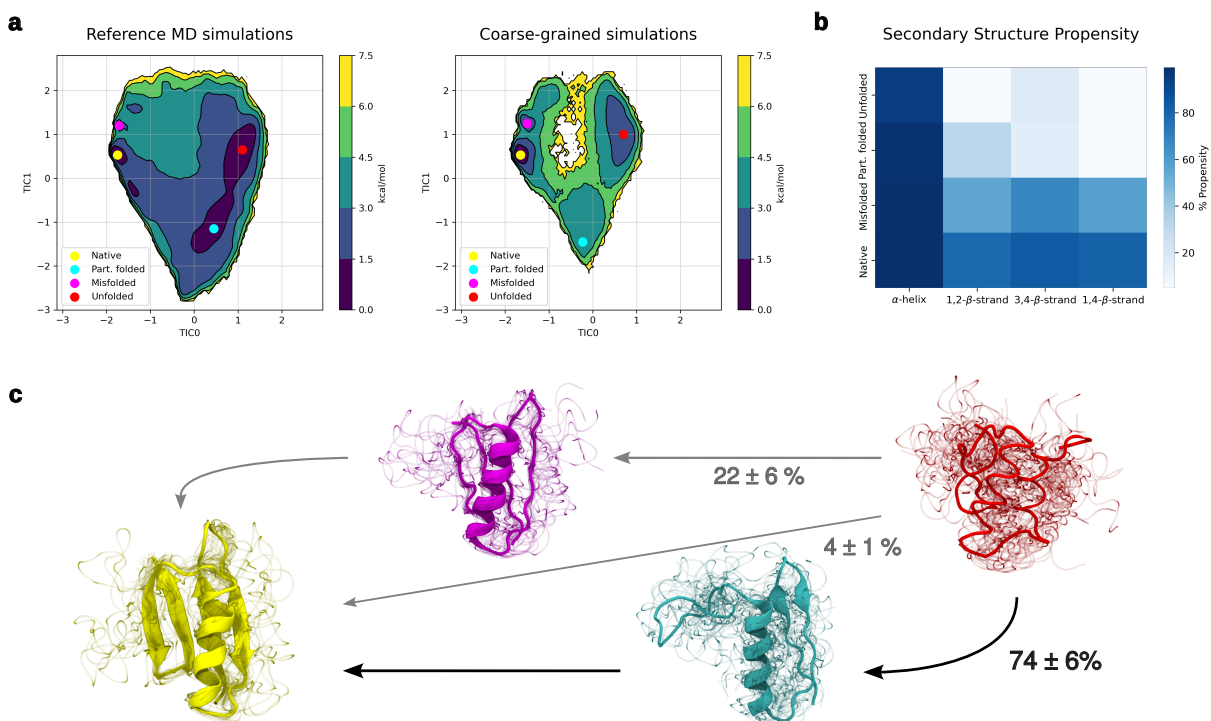


Figure 3: (a) Free energy surface of Protein G over the first two TICs for the all-atom MD simulations (top) and the coarse-grained simulations (bottom) using the protein-specific model. The circles identify different relevant minima (yellow - native, magenta - misfolded, cyan - partially folded, red - random coil). (b) The propensity of all the secondary structural elements of Protein G across the different macrostates, estimated using an RMSD threshold of  $2\text{\AA}$  for each structural element shown in the x-axis. (c) Sampled conformations from the macrostates of coarse-grained simulations corresponding to the marked minima in the free energy surfaces in (a). Sampled structure colors correspond to the minima colors in the free energy surface plot, with blurry lines of the same color showing additional conformations from the same state. Arrows represent the main pathways leading from the random coil to the native structure with the corresponding percentages of the total flux of each pathway.

identify all of the native macrostates for protein-specific models described in the previous section, and in nine out of ten cases (excluding NTL9 and WW-Domain) where the general model sampled the native structure. In general, the general model neglects energetic barriers and overestimates the global minima, which leads to some trajectories being “stuck” at the native structure (Supporting Fig. 4 and 2).

In the cases of NTL9 and WW-Domain, the native structure is sampled only as an artefact of starting positions being equally distributed on the reference free energy surface (Supporting Fig. 1). The native structure is not stable as all simulations move quickly to unstructured conformations. For Protein G, simulations show that the native conformation is stable, but we could not sample any transitions into this conformation from random coil

initial conditions, although we could capture unfolding events. In these cases, the native structure is identified as the lowest energy structure by the NNP. Therefore we can promote transitions to the low-energy states by lowering the temperature of the simulation. We simulated these systems at temperatures of 300K and 250K. This approach showed that the NNP recovers the native structure of NTL9 at 300K. For Protein G and WW-Domain, lowering the temperature stabilizes conformations that resemble the experimental structures, but we have not observed transitions from fully disordered to ordered structures (Supporting Fig. 7).

One aspect that the failed cases have in common is the presence of  $\beta$ -sheets, which could be the reason why the general models make the proteins’ structured states unstable. Ten out of

twelve proteins in the training set contain  $\alpha$ -helices, with only Chignolin and WW-domain representing completely  $\beta$ -sheet proteins and BBA, NTL9 and Protein G containing a mix of secondary structure elements. Therefore, the general model might be biased towards helical structures. Another explanation could be that due to the locality of interactions  $\alpha$ -helices may be easier to learn for the NNP. Additionally, for all the helical proteins, the general model performs similarly to the protein-specific models (Table 2). In some cases, the frequency of transitions between states is altered, as well as the stability of the macrostates, but both models successfully recover the native conformations.

In the case of Trp-Cage, the general potential outperforms the protein-specific model. The location and the shape of the global minimum match better the reference simulations as well as experimental data, which indicates that the model benefits from additional data from other proteins (Supporting Fig. 4 and 2). In the case of Protein B, the general model also outperforms the protein-specific one, as it is able to improve the average RMSD of the native macrostate and samples the correct location of the experimental structure, although it is not detected as a minimum.

The results obtained with the general model show that our approach could scale to create a general-use CG force field. This model was able to simulate the transition from random coil to the correct native conformation for almost all target proteins, with the exception of  $\beta$ -sheet proteins (WW-Domain, NTL9 and Protein G), which required simulations at lower temperatures to recover the native state.

**The general NNP recovers the native structure of mutated proteins.** To further test the general NNP and assess its predictive power we simulated mutants of the originally targeted proteins. All mutants were sourced from PDB and the mutations did not affect the native structure of the target. Supporting Table 4 summarizes the structures selected for the experiment. For each mutant, we initially performed a CG simulation of a single trajectory that started from the native structure using the general model. In the majority of cases,

the structure immediately transitioned to a random coil. The mutants that kept the native conformation for 1 ns were further evaluated using the same protocol we used for the previous CG simulations.

The results show that the general CG model is able to recover the native conformation for all cases that succeeded in the initial validation, except one (Protein B mutant 2N35), with reasonably low RMSD values (Table 3, Supporting Fig. 8). Although the NNP was able to simulate the protein dynamics, the exploration of conformational space was limited, as the simulations converge rapidly to the native structure or the conformations resembling it. These cases demonstrate some ability of the general model to generalize outside of the training set even with a narrow training set of only twelve proteins.

All the examples that recovered the native conformation had very few mutations and were solely helical structures, for which the general model performs well. In the case of a mutant of Protein B (PDB: 2N35), the NNP failed to obtain the native structure. Its sequence contains 10 mutated residues, which may exceed the capacity of the model to generalize outside of the training set. As shown in Supporting Table 4, an increased number of mutations reduces the stability of the native macrostate. In the case of  $\beta$ -sheet containing proteins, even with a point mutation, the model failed to recover the native structure and the amino-acid chains immediately formed unstructured bundles. This observation is not surprising, given the difficulties encountered by the general model on the  $\beta$ -sheet containing targets.

Overall, the mutagenesis tests have shown limited but encouraging results for the predictive capabilities of the general model. Despite its failure to keep the native conformation stable for the sequences that are substantially altered or for proteins that contain  $\beta$ -sheets, the NNP recovered native macrostates of  $\alpha$ -helical proteins with minor changes in the sequence. This shows some capacity of the model to generalize.

## Conclusion

In this work, we combined coarse-graining with NNPs to model protein dynamics. We initially

Table 2: Native macrostate statistics from all MSMs built with CG simulations from all protein-specific models and the general multi-protein-trained model. The data describes the identified native macrostate for each protein, showing equilibrium probabilities in percentage (Macro prob.), average (with standard deviation) and minimum RMSD values with respect to the experimental structure and maximum GDT score values.

Protein	Protein specific				General			
	Macro prob. (%)	Mean RMSD (Å)	Min RMSD (Å)	Max GDT	Macro prob. (%)	Mean RMSD (Å)	Min RMSD (Å)	Max GDT
Chignolin	19.7 ± 0.8	0.7 ± 0.4	0.2	100	33.4 ± 0.6	1.2 ± 0.6	0.2	100
Trp-Cage	93.2 ± 0.7	2.8 ± 0.5	1.0	91	81.1 ± 12.0	2.9 ± 0.5	1.0	90
BBA	41.1 ± 1.8	3.8 ± 1.0	1.6	82	17.5 ± 1.4	4.4 ± 1.0	1.6	85
WW-Domain	15.4 ± 2.5	2.5 ± 0.5	1.1	92	—	—	—	—
Villin	77.3 ± 8.9	2.7 ± 0.9	0.8	96	77.7 ± 13.0	2.9 ± 0.9	1.0	92
NTL9	32.0 ± 2.2	2.4 ± 0.9	0.6	99	—	—	—	—
BBL	95.0 ± 0.5	2.8 ± 1.2	1.0	78	47.8 ± 8.3	2.4 ± 0.6	0.9	77
Protein B	71.6 ± 1.6	5.6 ± 1.0	2.3	69	75.8 ± 6.4	3.3 ± 0.5	2.0	73
Homeodomain	77.6 ± 14.0	2.8 ± 0.4	1.8	67	98.5 ± 0.4	2.4 ± 0.3	1.5	71
Protein G	64.8 ± 3.9	2.7 ± 0.5	1.4	87	2.1 ± 0.9	2.2 ± 0.4	1.2	88
α3D	90.5 ± 6.9	3.2 ± 0.2	2.4	65	96.4 ± 2.4	3.4 ± 0.3	2.2	70
λ-repressor	77.4 ± 10.7	4.3 ± 0.5	2.1	69	79.1 ± 7.0	4.6 ± 0.7	2.8	65

Table 3: Native macrostate statistics of mutant variants of the proteins based on the CG simulations performed with the general multi-protein-trained model. The table shows the protein name, PDB ID and the number of amino acid substitutions for each mutant. Results show the minimum RMSD with respect to the mutant experimental structure, as well as the mean RMSD and equilibrium probability of the native macrostate, obtained from an MSM built based on CG simulations of the mutant.

Protein	PDB	Number of Substitutions	Min RMSD (Å)	Mean RMSD (Å)	Eq. prob. (%)
BBL	1BAL	3	1.5	3.9 ± 0.9	52.3 ± 1.4
Protein B	1GAB	2	2.3	4.9 ± 1.2	32.5 ± 1.4
Protein B	2N35	10	4.0	9.3 ± 1.4	19.4 ± 0.8
Homeodomain	1DU0	1	1.6	2.6 ± 0.4	57.0 ± 3.2
Homeodomain	1P7I	1	1.4	2.5 ± 0.3	92.2 ± 13.3
Homeodomain	1P7J	1	3.8	4.6 ± 0.3	16.6 ± 6.6
Homeodomain	2HOS	4	1.6	3.1 ± 0.8	65.4 ± 5.7
Homeodomain	6M3D	2	1.5	2.5 ± 0.3	24.5 ± 4.0
α3D	2MTQ	3	2.8	4.4 ± 0.6	96.2 ± 0.9
λ-repressor	1LLI	3	3.1	5.1 ± 0.9	97.0 ± 0.8
λ-repressor	3KZ3	6	2.3	5.8 ± 1.4	76.1 ± 7.6

generated a multi-millisecond dataset of MD simulations sampling the dynamical landscape of twelve structurally diverse proteins. We used it to obtain machine-learned CG potentials for studying the protein dynamics, extending previous studies on learning CG models to much larger and more complex proteins. Results show that we were able to model protein dynamics in computationally accessible timescales, and recover the native structure of all twelve proteins through coarse-grained MD simulations using NNPs and an  $\alpha$ -

carbon CG representation, with a unique bead type corresponding to each amino-acid type. From the model-generated CG simulation data, we were able to reconstruct multiple metastable states, capturing the folding pathways and the formation of different types of secondary and tertiary structures. In contrast to novel deep-learning structure prediction methods,<sup>74,75</sup> our method offers a substantial improvement and models protein dynamics, which is essential for understanding protein function. The general model, trained over all proteins in the MD dataset, represents a step forward towards making NNPs transferable across molecular systems. Additionally, the mutagenesis study indicates that with a much larger and structurally diverse set of MD data, this approach might produce a general-use CG model capable of generalizing outside of its training set.

There are a few limitations to the current approach. In general, machine learning potentials do not extrapolate well outside of the training set for atom positions that are never sampled in the training set. Therefore, unseen positions are assigned unrealistically low energies and often produce spikes in forces. This has been solved by limiting the physical sampled space with the use of basic prior energy terms.<sup>43</sup> The network also relies on large datasets of all-atom molecular dynamics trajectories which are expensive to produce. Furthermore, the current accuracy of coarse-grained MD is limited by the accuracy of the underlying all-atom simulations. While all-atom force-

fields are reasonably good for proteins, improved approaches are required for coarse-grained small molecules.<sup>76</sup> Ultimately, the ability to create a general model that is transferrable from smaller to larger proteins would revolutionize the field. However, in order to learn transferable potentials, even larger molecular simulation datasets are needed. Current results indicate that this might be achievable.

## Materials and Methods

### All-atom molecular dynamics simulations and training data.

All initial structures were solvated in a cubic box and ionized as described by Lindorff-Larsen *et al.*<sup>8</sup> MD simulations were performed with ACEMD<sup>77</sup> on the GPU GRID.net distributed computing network.<sup>78</sup> The systems were simulated using the CHARMM22\*<sup>79</sup> force field and TIP3P water model<sup>80</sup> at the temperature of 350K. All the simulations were performed following a previously used adaptive sampling strategy,<sup>81</sup> in order to explore efficiently as many conformations as possible. Homeodomain dataset also contains simulations that started from the native conformation, as low RMSD values ( $\leq 2\text{\AA}$ ) with respect to the native structure are difficult to sample when starting from random coil conformations. A Langevin integrator was used with a damping constant of  $0.1\text{ ps}^{-1}$ . Integration time step was set to 4 fs, with heavy hydrogen atoms (scaled up to four times the hydrogen mass) and holonomic constraints on all hydrogen-heavy atom bond terms.<sup>82</sup> Electrostatics were computed using Particle Mesh Ewald with a cutoff distance of 9 Å and grid spacing of 1 Å. Ten NVT simulations of 1 to 10 ns length were carried out for each protein, with a dielectric constant of 80 and temperature of 500 K to generate ten different starting random coil conformations for the production runs. Production simulations consisted of thousands of short trajectories of 20, 50 or 100 ns, distributed across different epochs using the adaptive sampling<sup>81,83</sup> protocols implemented in HTMD.<sup>84</sup> In adaptive sampling, multiple rounds of simulations are performed, and in each round the available trajectories are analyzed to select the initial coordinates for the next

round of simulations. The MSM constructed during the analysis was done using atom distances, using TICA for dimensionality reduction and k-centers for clustering. From the trajectories, we extracted forces and coordinates with an interval of 100 ps. Total aggregate times used for training for all the proteins are summarized in Table 1.

Based on the MD dataset we built MSMs for each protein. The models were able to describe the conformational dynamics of each protein, sample the native conformation and identify intermediate and metastable states for some of them, such as Villin, NTL9, WW-Domain or Protein G (Supporting Fig. 2).

**Neural network training.** To train NNPs we used TorchMD-Net.<sup>76</sup> More details on the network and training can be found in Supporting Information. We performed an exhaustive hyperparameter search, which is described in the Supporting Table 1. The data was randomly split between training (85%), validation (5%) and testing (10%). An epoch for simulation was selected when the validation loss reached a minimum or a plateau. To ensure the reproducibility of the results, the training of each model was repeated 2 to 4 times with different random seeds. Each replica was then tested by performing a fast simulation of 4 parallel trajectories of a corresponding system, with the objective of a fast assessment of the model. The model that produced the best results was selected for the main validation. The training, validation and test loss as well as learning rates of models selected for simulation are presented in Supporting Figure 3 and 6. The models were trained using Nvidia GeForce RTX 2080 graphics cards. The training of protein-specific models took from 7 min/epoch on a single GPU for Chignolin to 24 min/epoch on 2 GPUs for  $\lambda$ -repressor. The training of the general model took 46 min/epoch on 3 GPUs.

**Coarse-grained simulations.** Coarse-grained representations were created by filtering all-atom coordinates such that only certain atoms are retained. This mapping is a simple linear selection, wherein the mapping matrix that transforms the all-atom coordinates to the coarse-grained coordinates is a matrix where zero-entries filter out unwanted beads. The all-atom trajectories were filtered to retain the coordinates and forces of  $\alpha$ -carbon atoms (CA). To speed up the training, tra-



jectories were further reduced by selecting every 10<sup>th</sup> frame. However, for smaller proteins (Chignolin, Trp-Cage, BBA and Villin), the training data was not sufficient to produce satisfactory models. Therefore all the frames were used in the training of these systems. Each CA bead was assigned a bead type based on the amino acid type. In the assignment we ignored the protonation states and distinguished norleucine, a non-standard residue appearing in Villin, as a unique entity. As a result, we obtained 21 unique bead types. To each bead type we assigned a unique integer, an embedding that will be used as an input for the network.

To perform the coarse-grained simulations using a trained NNP, we used TorchMD,<sup>62</sup> an MD simulation code written entirely in PyTorch.<sup>85</sup> The package allows for an easy simulation with a mix of classical force terms and NNPs. The parameters for the prior energy terms were enumerated and stored in YAML files, described in Supporting Information. The NNP was introduced as an external force, as described in the previous work.<sup>62</sup> We carried out CG simulations over all the proteins, both for each protein-specific model and for the general model, as well as selected mutants. Simulations were set up with a configuration file (an example in Supporting Listing 2). We selected 32 conformations evenly distributed across the free energy surface of the reference simulations from where to start the coarse-grained simulations (Supporting Fig. 1). For each system, 32 parallel, isolated trajectories were run at 350 K for the time necessary to observe transitions between states with a 1 fs time step, saving the output every 100 fs. The length of each individual trajectory was 1.56 ns (accumulated time of 50 ns) for Chignolin and BBA, 3.12 ns (accumulated time of 100 ns) for Trp-Cage and Villin, 12.5 ns (accumulated time of 400 ns) for WW-Domain and Protein G, and 6.25 ns (accumulated time of 200 ns) for the remaining protein targets. For some systems and models, we were able to obtain stable trajectories with a time step as high as 10 fs. However, to make the results comparable we adapted identical parameters for all simulations, and thus we were limited by the highest possible time step where all types of simulations were stable (1 fs). The coarse-grained simulations were performed using Nvidia GeForce RTX 2080 graphics cards.

**Markov state model estimation and structure selection.** For the analysis of the CG simulations and their comparison with the all-atom MD simulations, we built MSMs for each protein, both for the all-atom MD simulations and the two sets of coarse-grained simulations (protein-specific and general models). The basic concept behind MSMs is that the dynamics of the system are modeled as a memory-less jump process, where future states are only conditioned on the current state, hence the dynamics are Markovian. MSM estimation of transition rates and probabilities requires partitioning the high-dimensional conformational space into discrete states. In order to project the high-dimensional conformational space into an optimal low-dimensional space, we use TICA, a linear transformation method that projects simulation data into its slowest components by maximizing autocorrelation of transformed coordinates at a given lag time.<sup>69,70</sup> The resulting low-dimensional projected space is then discretized using a clustering algorithm for the MSM construction.

For the all-atom MD simulations, we featurized the simulation data into pairwise  $C_\alpha$  distances and applied TICA to project the featurized data into the first 4 components. Next, the components were clustered using a K-means algorithm and the discretized data was used to perform the MSM estimation. Although better reference MSM models could be obtained by using different featurizations, we are limited to only using pairwise  $C_\alpha$  distances as it is transferable between systems and comparable with the coarse-grained simulations.

For the coarse-grained simulations, the same procedure was used. However, when projecting the featurized data into the main TICs, we used the covariance matrices computed with the all-atom MD simulations to project the first 3 components, in order to compare how well the coarse-grained simulations reproduce the free energy surface for each protein. For each MSM, we used the PCCA algorithm to cluster microstates into macrostates for better interpretability of the model and to define a native macrostate that we can use to evaluate the performance of the coarse-grained simulations. To avoid biasing the model with starting conformations, we removed 10% of the initial frames of each trajectory from the analysis.

The free energy surface plots used for compar-

ison were obtained by binning over the first two TICA components, dividing them into an  $80 \times 80$  grid, and averaging the weights of the equilibrium probability in each bin, obtained for each defined microstate through MSM analysis. To recover the native conformation from a set of coarse-graining simulations, we used the MSMs and sampled 10 conformations from the native macrostate. The native macrostate was defined as the macrostate containing the frame with the minimum RMSD to the experimental structure.

**Code, models and data availability.** All codes are free available in [github.com/torchmd](https://github.com/torchmd). The neural network architecture is available at [github.com/torchmd/torchmd-net](https://github.com/torchmd/torchmd-net). The models, data and tutorials to reproduce this work are available at [github.com/torchmd/torchmd-protein-thermodynamics](https://github.com/torchmd/torchmd-protein-thermodynamics).

# 1 Supporting Information

## Neural network optimization and hyper-parameters

A lot of effort was dedicated to building a graph neural network architecture TorchMD-GN, inspired by SchNet<sup>55,86</sup> and PhysNet<sup>56</sup> and optimized to work optimally on noisy forces and energies proper of the reduced dimensionality of our coarse-graining. This scenario is different from the quantum case, where energy and forces are deterministic functions of the coordinates. In coarse-grained systems, the same coordinates generate stochastic energies and forces. The software was implemented using PyTorch Geometric<sup>87</sup> and PyTorch lightning framework<sup>88</sup> and is publicly available in TorchMD-Net.<sup>76</sup> The SchNet architecture has several distinct components, each playing an important function in predicting system forces and energies for given input configurations. The formal inputs into the network are the Cartesian coordinates for a full configuration and a predetermined type for each coarse-grain bead. In the first network operation, a molecular graph,  $\mathcal{G}$ , is constructed, where each coarse grain bead represents a node. Each node is given an embedding feature vector, the set of which is grouped into a feature tensor. For SchNet, the embedding is produced by applying a learnable linear mapping. The edges of  $\mathcal{G}$  are used to define the network operations that update the features of each node. These updates are encompassed in so-called *interaction blocks*, which are a form of message-passing updates. The edges of  $\mathcal{G}$  are the set of pairwise distances for each bead from its nearest neighbors, the range of which is set uniformly for all beads by an upper cutoff distance. In this way, several interaction blocks can be stacked in succession to give the network increased expressive power. After the final interaction block, an output network is used to contact the node feature dimension to a scalar for each node. This forms a set of scalar energy predictions,  $U$  from each node. By applying a gradient operation with respect to the network input coordinates, the curl-free Cartesian forces,  $F$ , are predicted for each bead, representing the final network output.

The hyperparameters were selected based on the quality of the simulation produced using protein-specific models. An example of a training input file is presented in Supporting Listing 1. The test loss was not a useful metric for hyperparameter selection because the value did not change much between successful and failed models. The only way to correctly validate the models was to use them in coarse-grained simulations. The biggest influence on the results was found to be the number of interaction layers, the type, range and number of radial base functions, and the type of activation function. Based on the results for protein-specific models as well as the general model, we selected the following combination: 4 interaction layers, 128 filters used in continuous-filter convolution, 128 features to describe atomic environments, and 18 expnorm as radial base functions (RBF) span in the range from 3.0 to 12.0 Å. The Gaussian function that was used in previous works, expnorm is slightly elongated towards longer distances and this shape might better suit modelling the properties of CG beads. We have found that this type of RBF is improving the stability of simulations and produces results of better quality.

## Neural network architecture

The series of full network operations can be written as:

$$\xi^0 = W^E z \quad (2)$$

$$\xi^1 = \xi^0 + W^0 \sigma (\text{Aggr}(W^C * \xi^0)) \quad (3)$$

$$\xi^2 = \xi^1 + W^1 \sigma (\text{Aggr}(W^C * \xi^1)) \quad (4)$$

$$\vdots \quad (5)$$

$$\xi^N = \xi^{N-1} + W^{N-1} \sigma (\text{Aggr}(W^C * \xi^{N-1})) \quad (6)$$

$$U = H_{out}(\xi^N) \quad (7)$$

$$F = -\text{grad}(U, x) \quad (8)$$

for  $N$  interaction blocks. Note that for clarity, we have omitted learnable additive biases in all linear operations above, though they are easily incorporated. The first step of the message-passing update involves expanding the pairwise distances into a set of radial basis functions,  $\phi$ .  $\phi$  then comprises a "filter generating network" used to produce a set of continuous filters,  $W^C$ :

$$W^C = W_2(\sigma(W_1\phi)) \quad (9)$$

where  $W_1, W_2$  are learnable linear weights and  $\sigma$  is an element-wise non-linearity. These filters are used in a continuous filter convolution through an element-wise multiplication with the current node features for  $\mathcal{G}$ . These convolved features are then passed through a non-linearity and added directly to the unconvolved node features through a residual connection:

$$\xi^{i+1} = \xi^i + W^i \sigma (\text{Aggr}(W^C * \xi^i)) \quad (10)$$

where "Aggr" is a chosen pooling/aggregation function that reduces the convolution output (eg, sum, mean, max, etc.). This message-passing update, combined with the residual connection, forms the entirety of an interaction block, producing an updated set of node features for  $\mathcal{G}$  that can be used as input for another interaction block. Our implementation of this network architecture allows for training on multiple GPUs and more efficient utilization of GPU memory.

## Prior energy terms

The pairwise bonded term was represented with the following equation:

$$V_{harmonic}(r) = k(r - r_0)^2 + V_0, \quad (11)$$

where  $r$  is the distance between the beads forming the bond,  $r_0$  is the equilibrium distance,  $k$  is the spring constant and  $V_0$  is a base potential. The nonbonded repulsive term was represented by the potential

$$V_{repulsive}(r) = 4\epsilon r^{-6} + V_0, \quad (12)$$

where  $\epsilon$  is a constant that was fit to the data,  $r$  is the distance between the beads and  $V_0$  is a base potential. The parameters were used as in TorchMD.<sup>62</sup> The parameters for norleucine, a non-standard residue appearing in Villin, were adapted from leucine. Additionally, We introduced a third prior dihedral term:

$$V_{dihedral}(\phi) = \sum_{n=1,2} k_n(1 + \cos(n\phi - \gamma_n)), \quad (13)$$

where  $\phi$  is the dihedral angle between the four consecutive beads,  $k_n$  is the amplitude and  $\gamma_n$  is the phase offset of the harmonic component of periodicity  $n$ . The parameters for dihedral terms were fit to the data used for training, containing all the proteins. The extracted values of  $k_n$  were scaled by half to achieve a soft prior that will break the symmetry in the system but will not disturb the simulation in a major way. For simplicity, all combinations of four beads were treated equally, therefore all dihedral angles were characterised by the same set of parameters, in contrast to bonded and repulsive prior. The force field file with terms and associated parameters is available as a part of Supporting Information. To enable the simultaneous use of both Dihedral and RepulsionCG force terms in TorchMD, exclusions between pairs of beads for RepulsionCG term are defined by an additional parameter 'exclusions'.

Table 1: Hyperparameter choices for the NNP training. The values selected for the final model are bolded. The rest of the parameters available in TorchMD-Net, that are not listed here, were left at default values. The number of RBF was listed as a range, as we tested a large number of different values, ultimately selecting 18.

Hyperparameter	Name	Values tested
Number of interaction layers	num_layers	[1,2,3, <b>4</b> ,5,6]
Activation function	activation	[ <b>tanh</b> , ssp]
Radial base function (RBF) type	rbf_type	[gauss, <b>expnorm</b> ]
Number of RBF	num_rbf	[2-150], <b>18*</b>
Upper cutoff for RBF	cutoff_upper	[4.0, 6.0, 9.0, <b>12.0</b> , 15.0]
Lower cutoff for RBF	cutoff_lower	[0.0, <b>3.0</b> , 3.6, 4.1]
Trainable RBF	trainable_rbf	[ <b>true</b> , false]
Model type	model	graph-network
Embedding dimension	embedding_dimension	[ <b>128</b> , 256]
Early stopping patience	early_stopping_patience	30
Initial learning rate (LR)	lr	0.0005
LR factor	lr_factor	0.8
Minimal value of LR	lr_min	1.0e-06
LR patience	lr_patience	10
Number of LR warm up steps	lr_warmup_steps	0
Neighbor embedding	neighbor_embedding	false
Saving interval	save_interval	2
Testing interval	test_interval	2
Test set ratio	test_ratio	0.1
Validation set ratio	val_ratio	0.05
Weight decay	weight_decay	[ <b>0.0</b> , 0.1, 0.001]
Force Terms	-	<b>Bonds, Angles, Dihedrals, RepulsionCG</b>

Listing 1: Input file with a set of hyperparameters used for training of the general network. The protein-specific networks were trained with the same set of hyperparameters, with the exception of the fields "coord\_files", "embed\_files" and "force\_files", which were set to the files appropriate for each protein target, and "num\_epochs", which was set to 200.

```

activation: tanh
batch_size: 256
inference_batchsize: 256
dataset: Custom
coord_files: "data/*coords*.npz"
embed_files: "data/*embeddings.npz"
force_files: "data/*deltaforces*.npz"
cutoff_upper: 12.0
cutoff_lower: 3.0
derivative: true
distributed_backend: ddp

```

```
early_stopping_patience: 30
embedding_dimension: 128
label:
- forces
lr: 0.0005
lr_factor: 0.8
lr_min: 1.0e-06
lr_patience: 10
lr_warmup_steps: 0
model: graph-network
neighbor_embedding: false
ngpus: -1
num_epochs: 100
num_layers: 4
num_nodes: 1
num_rbf: 18
num_workers: 8
rbf_type: expnorm
save_interval: 2
seed: 94572
test_interval: 2
test_ratio: 0.1
trainable_rbf: true
val_ratio: 0.05
weight_decay: 0.0
```

Listing 2: An example of simulation input file.

```
forcefield: ca_priors-dihedrals-general.yaml
forceterms:
- Bonds
- RepulsionCG
- Dihedrals
exclusions: ('bonds')
langevin_gamma: 1
langevin_temperature: 350
log_dir: cln_32trajs_350_ts1
output: output
output_period: 100
precision: double
replicas: 32
rfa: false
save_period: 1000
seed: 1
steps: 5000000
topology: cln.psf
coordinates: cln_kcenters_32clusters_coords.xtc
temperature: 350
timestep: 1
external:
```



```

module: torchmdnet.calculators.torchmdcalc
embeddings: [4, 4, 5, 8, 6, 13, 2, 13, 7, 4]
file: model.ckpt

```

Table 2: Sequences of the proteins used for training. (\*) In the sequence of Villin, “X” stands for the non-standard amino-acid norleucine (NLE).

Protein	Sequence
Chignolin	YYDPETGTWY
Trp-Cage	DAYAQWLKDGPPSSGRPPPS
BBA	EQYTAKYKGRTRFNEKELRDFIEKFKGR
WW-Domain	KLPPGWEEKRMSRSSGRVYYFNHITNASQWERPSG
Villin (*)	LSDEDFKAVFGMTRSAFANLPLWXQQHLXKEKGLF
NTL9	MKVIFLKDVKMGKKGKGEIKNVADGYANNFLFKQGLAIEA
BBL	GSQNNDALSPAIRLLAEWNLDASAIKGTGVGGRLTREDVEKHLAKA
Protein B	LKNAIEDAIAELKKAGITSDFYFNAINAKKTVEEVNALVNEILKAHA
Homeodomain	RPRTAFSSEQLARLKRREFNENRYLTERRRQQLSSELGLNEAQIKIWFQNKRAKI
Protein G	DTYKLVIVLNGTTFTYTTEAVDAATAEKVFKQYANDAGVDGEWYDAATKTFTVTE
$\alpha$ 3D	MGSWAEFKQRLAAIKTRLQALGGSEAEAAFEKEIAAFESELQAYKKGKGNPEVEALRKEAAAIRDELQAYRHN
$\lambda$ -repressor	PLTQEQLDARRLKAIEYKKNELGLSQESVADKMGMGQSGVGALFNGINALNAYNAALLAKILKVSVEEFSPSIAREIY

Table 3: Visualizations of representative trajectories, where each protein reaches the native state, generated using coarse-grained simulation with NNP. The selected trajectories correspond to trajectories selected in Figure 2 and Supporting Figure 5. The trajectories for WW-Domain, NTL9, BBL, Protein B and Protein G were split into parts, visualizing transitions between states and separated by 2 s of blank frames. The movies were produced with Open-Source PyMOL<sup>89</sup> with period of 0.5 ps per frame.

Protein	Trajectory	Time frame [ns]	Video URL
Chignolin	28	0.0 - 0.615	<a href="https://youtu.be/vs5jff_3VheA">https://youtu.be/vs5jff_3VheA</a>
Trp-Cage	16	1.49 - 2.6	<a href="https://youtu.be/l9MI6XQZjnU">https://youtu.be/l9MI6XQZjnU</a>
BBA	11	0.0 - 1.0	<a href="https://youtu.be/G9PnPkelL17E">https://youtu.be/G9PnPkelL17E</a>
WW-Domain	4	1.1 - 1.6 & 9.5 - 10.0	<a href="https://youtu.be/dBDOKvZ4CS4">https://youtu.be/dBDOKvZ4CS4</a>
Villin	14	2.08 - 2.5	<a href="https://youtu.be/beQVf8YEpxI">https://youtu.be/beQVf8YEpxI</a>
NTL9	28	3.4 - 3.9 & 4.5 - 5.0	<a href="https://youtu.be/CSOaCFcx0Ho">https://youtu.be/CSOaCFcx0Ho</a>
BBL	29	0.0 - 0.5 & 3.5 - 4.0	<a href="https://youtu.be/lwia6Z6ik9k">https://youtu.be/lwia6Z6ik9k</a>
Protein B	27	0.0 - 0.5 & 3.5 - 4.0	<a href="https://youtu.be/715Zavu25eg">https://youtu.be/715Zavu25eg</a>
Homeodomain	23	0 - 1.0	<a href="https://youtu.be/QG0gQJwvwxM">https://youtu.be/QG0gQJwvwxM</a>
Protein G	14	0.0 - 0.2 & 3.3 - 3.4 & 7.3 - 8.2	<a href="https://youtu.be/Ozt63Z9yB3w">https://youtu.be/Ozt63Z9yB3w</a>
$\alpha$ 3D	4	0.0 - 0.8	<a href="https://youtu.be/56LD1UbptpE">https://youtu.be/56LD1UbptpE</a>
$\lambda$ -repressor	20	0.0 - 1.1	<a href="https://youtu.be/0U10m_MgC7g">https://youtu.be/0U10m_MgC7g</a>

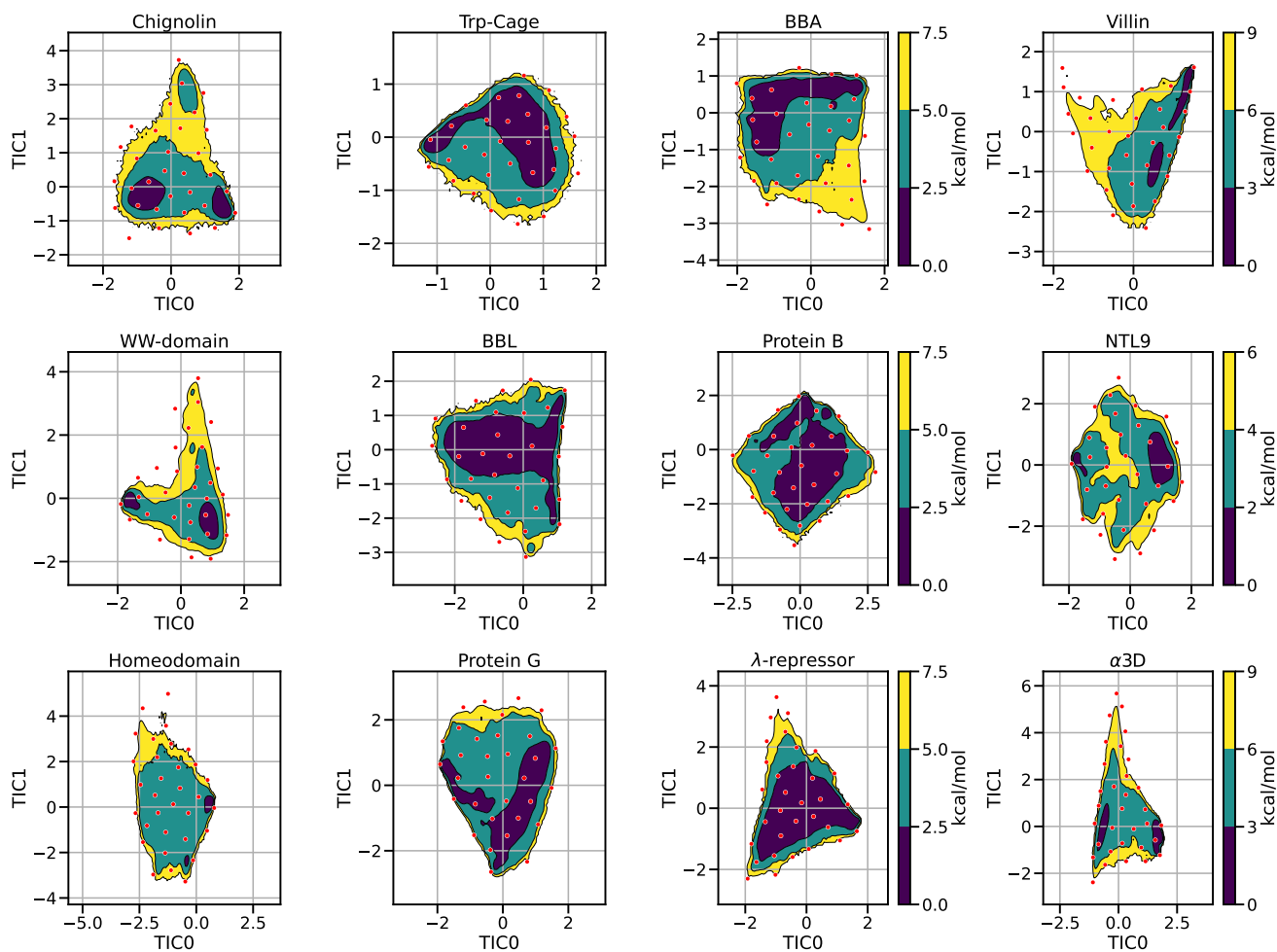


Figure 1: Starting points (red dots) of coarse grained molecular dynamics overlaid on top of free energy surface across the first two TICA dimensions for each protein. The colorbar shows the energy values in the range from 0 to 9 kcal/mol for Villin and  $\alpha$ 3D, 6 kcal/mol for NTL9, and 7.5 kcal/mol for the remaining proteins.

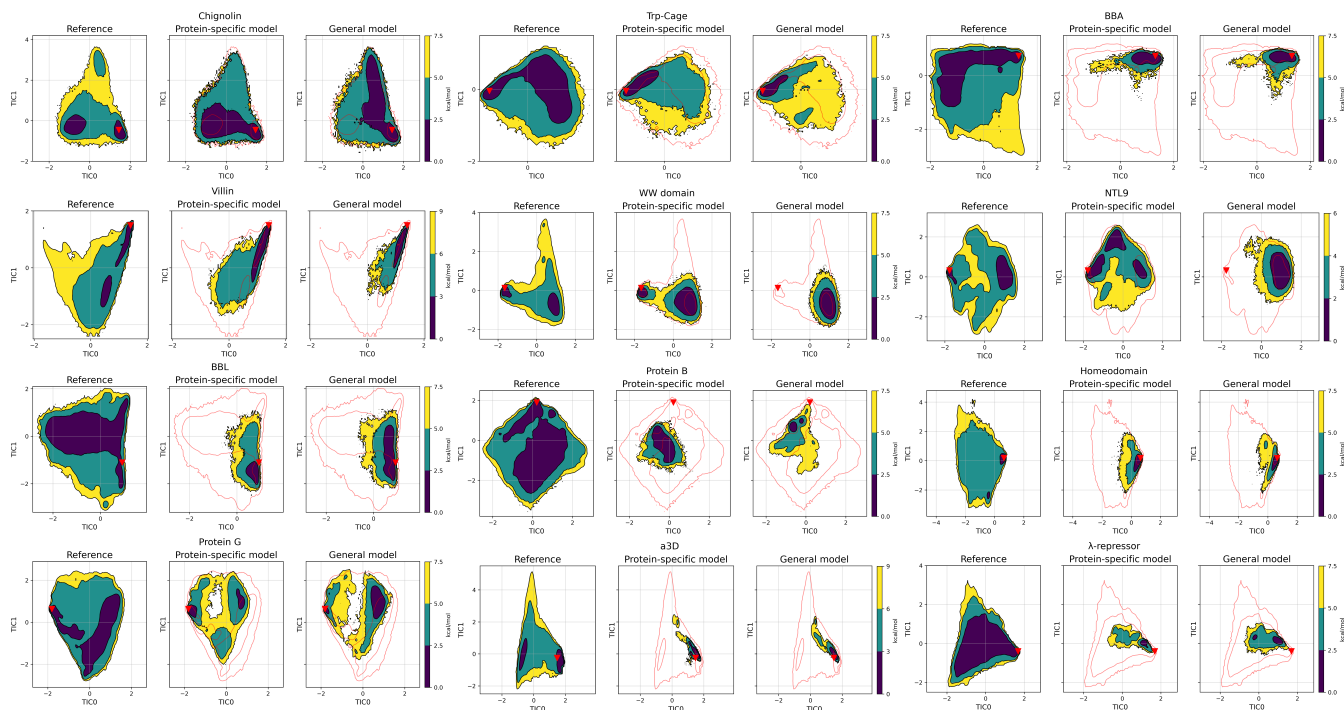


Figure 2: Comparison between the reference MD (left), protein specific model (center) and general model (right) coarse-grained simulations free energy surface across the first two TICA dimensions for each protein. The free energy surface for each simulation was obtained by binning over the first two TICA dimensions, dividing them into a  $80 \times 80$  grid, and averaging the weights of the equilibrium probability in each bin computed by the Markov state model. The red line indicates the all-atom equilibrium density by showing the energy level above free energy minimum with the values of 9 kcal/mol for Villin and  $\alpha 3D$ , 6 kcal/mol for NTL9, and 7.5 kcal/mol for the remaining proteins.

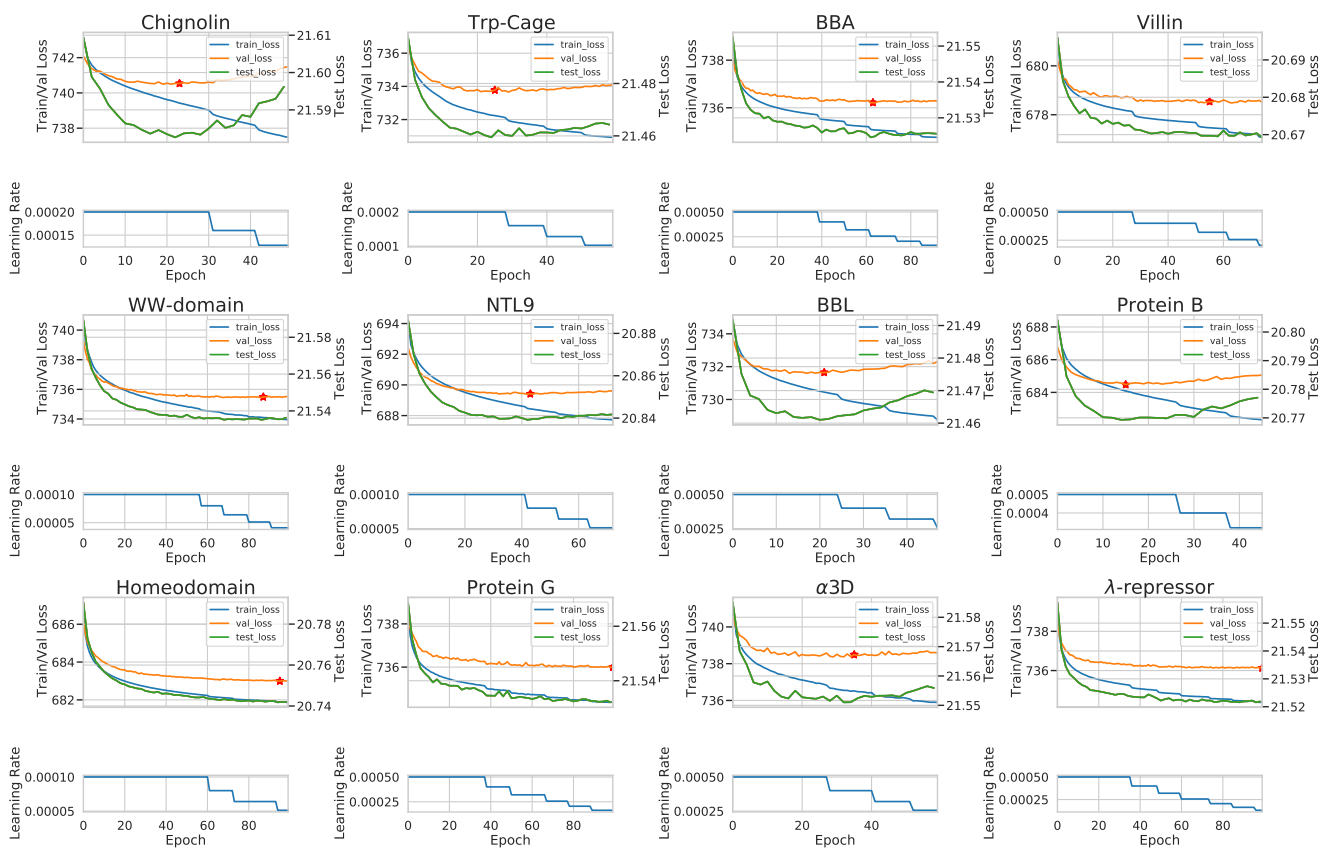


Figure 3: Training curves for the models trained on individual proteins. Top panel: training (blue, *train\_loss*), validation (orange, *val\_loss*) and test loss (green, *test\_loss*). Bottom panel: learning rate values across the training of the corresponding models. The models selected are marked with a red star.

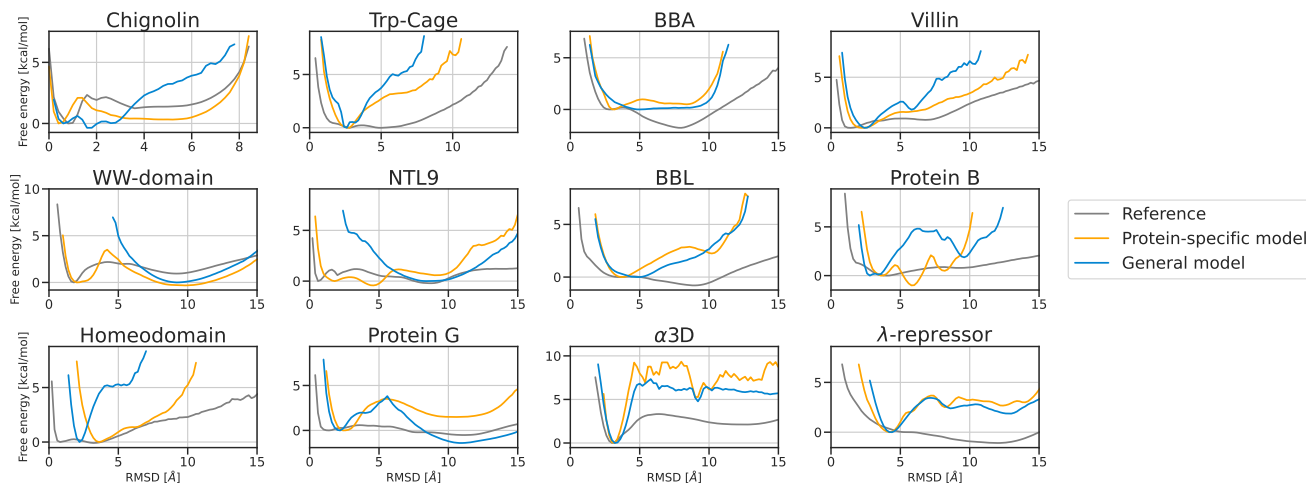


Figure 4: Free energy curve over  $C\alpha$ -RMSD for the all-atom MD and CG models with PDB structure as the reference. The reference PDB is listed on Figure 1.

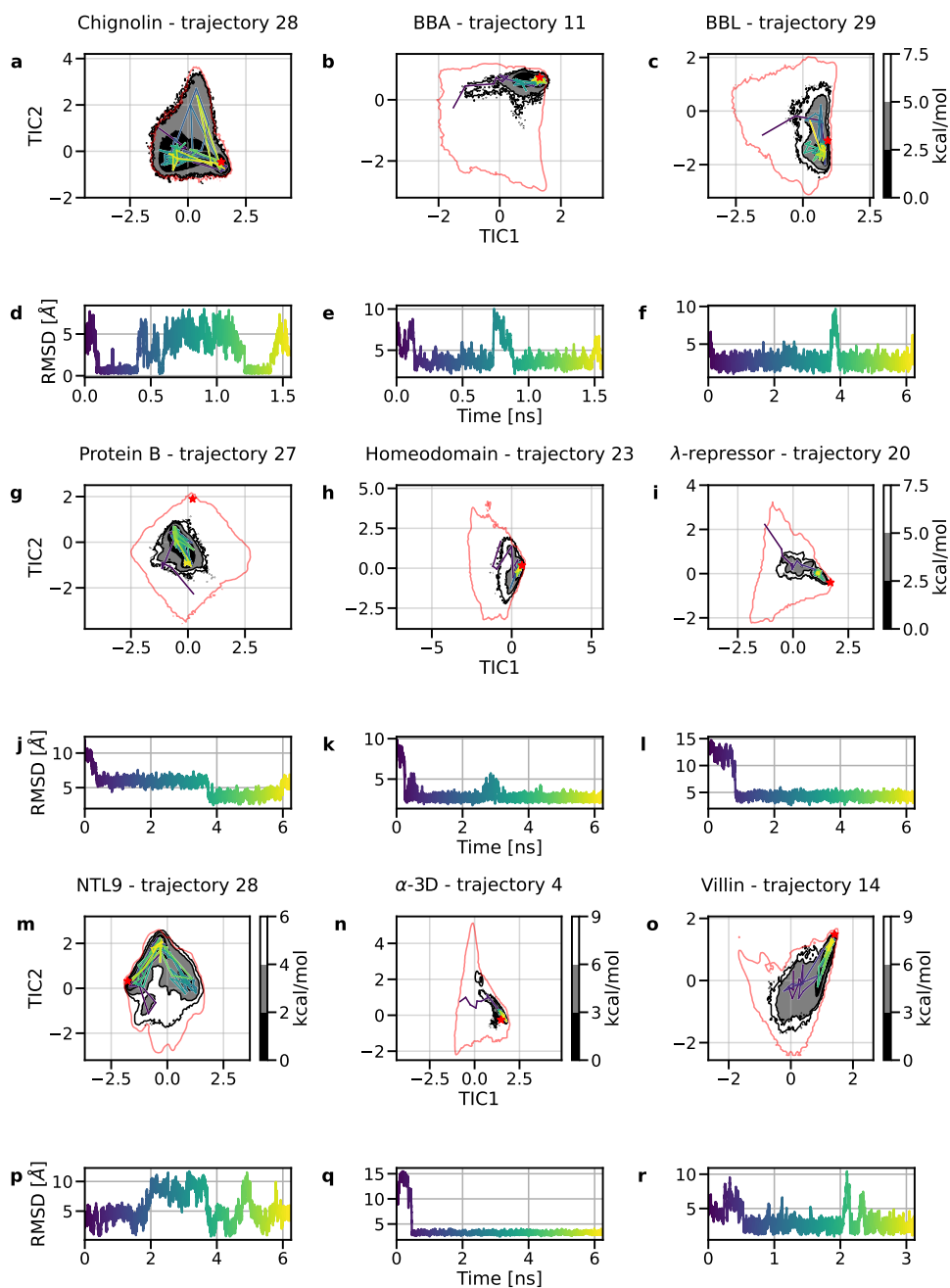


Figure 5: Individual CG trajectories selected for 9 of the proteins. Each visualized simulation explores the free energy surface, accesses multiple major basins and shows transitions between native and coil states. On the top panel of each sub figure: 100 states sampled uniformly from the trajectory plotted over CG free energy surface. The red line indicates the all-atom equilibrium density by showing the energy level above free energy minimum with the values of 9 kcal/mol for  $\alpha$ 3D, 6 kcal/mol for NTL9, and 7.5 kcal/mol for the remaining proteins. On the bottom panel: RMSD of  $\alpha$ -carbon with the reference to the crystal structure. The remaining proteins are included in Figure 2.

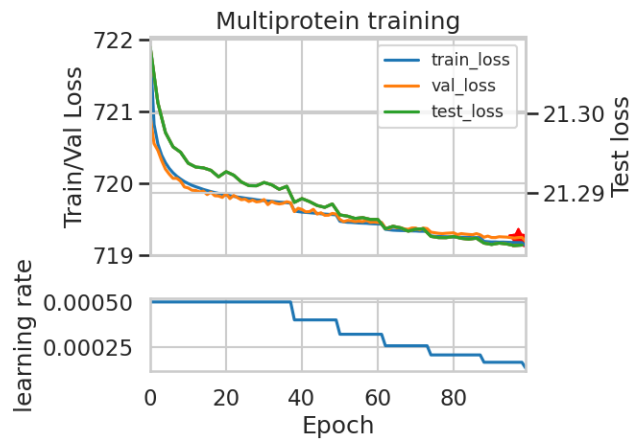


Figure 6: Training curves for the general model trained on all the proteins. Top panel: training (blue, *train\_loss*), validation (orange, *val\_loss*) and test loss (green, *test\_loss*). Bottom panel: learning rate values across the training of the corresponding models. The model selected is marked with a red star.



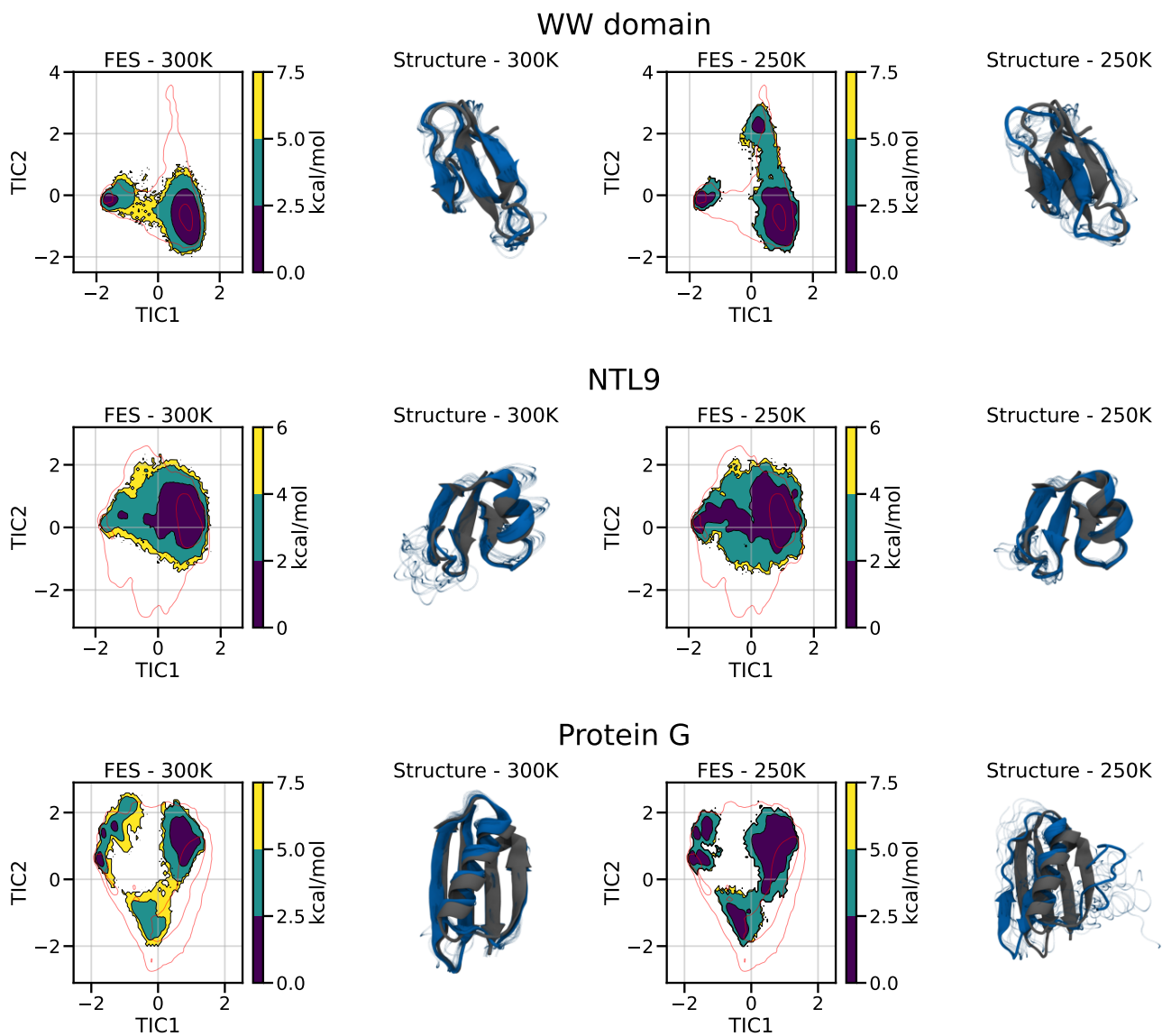


Figure 7: Results of CG simulation with the general model at lower temperatures (300K and 250K) for WW domain, NTL9 and Protein G. The results for each protein are presented in individual row from left to right: Free energy surface at 300K; Representative structure of the native macrostate at 300K; Free energy surface at 250K; Representative structure of the native macrostate at 250K.

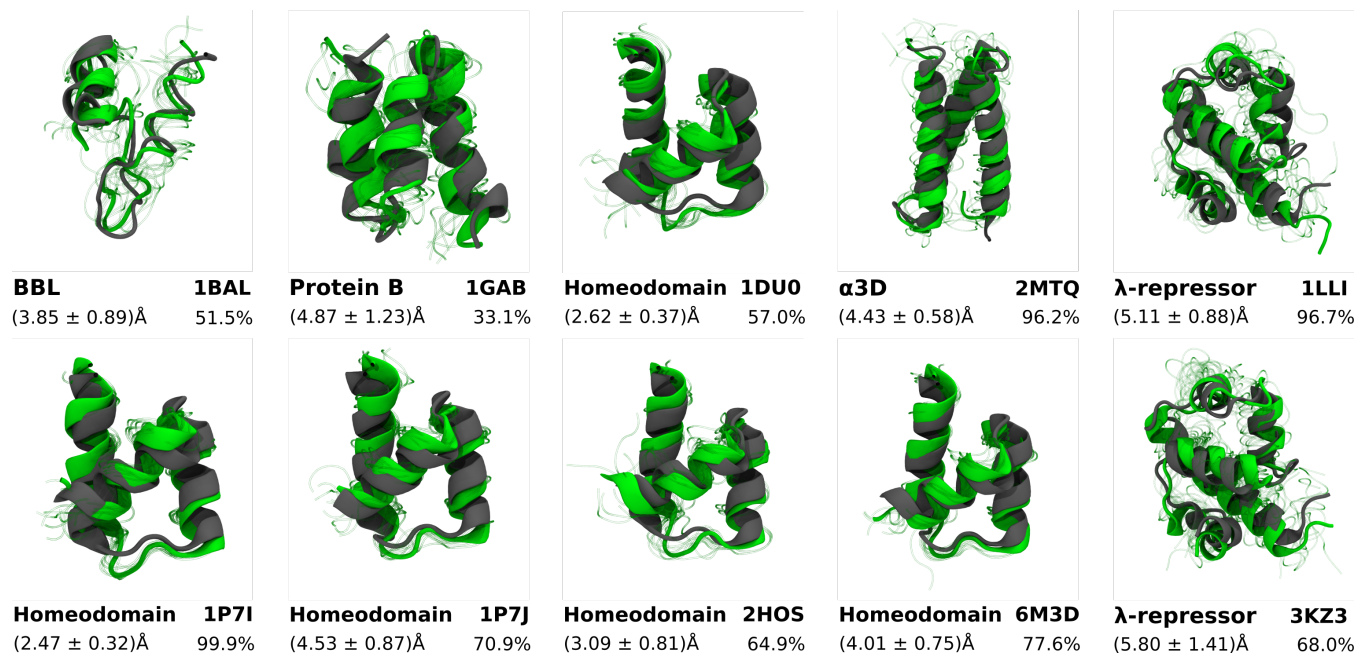


Figure 8: Representative structures for selected mutants retrieved from the CG simulations made from the general model. Structures were sampled from the native macrostate, which was identified as the macrostate containing the conformation with the minimum RMSD with the reference to the mutant's crystal structure. Ten conformations were sampled from the native macrostate, and the backbone was reconstructed for the most similar one to the crystal structure, for visual purposes. In grey, the reference crystal structure. In green, the sampled structure with the backbone reconstructed. The green blurry structures are the remaining structures sampled from the same macrostate. Text indicates protein name and PDB ID. Values on the left indicate the average RMSD of the native macrostate, and percentage shows its equilibrium probability.

Table 4: Summary of selected protein mutants. The mutants that kept the native structure in a preliminary validation are presented in Table 3. The structures of recovered native macrostates of mutants that sampled transition to native state are shown in Supporting Figure 8. Amino-acid substitutions in the sequences are bolded, insertions are underlined and deletions are marked as '-'.

Protein	PDB	# mutations	Kept native structure	Transition to native state	Sequence
Chignolin	1UAO	2	No	No	GYDPETGTWG
Trp-Cage	1L2Y	3	No	No	NLYIQWLKDGPPSSGRPPPS
BBA	1FSD	2	No	No	QQYTAKIKGRTRFNEKELRDFIEKFKGR
BBA	1PSV	8	No	No	KPYTARIKGRTFNEKELRDFLETFTR
NTL9	1CQU	1	No	No	MKVIFLKDVKGKGGKGEIKNVADGYANNFLKQGLAIEA
Protein B	1GAB	2	Yes	Yes	LKNAKEDAI AELKKAGITSDFYFNAINKAKTVEEVNALKNEILKAHA
Protein B	2N35	10	Yes	No	LKEAKEKAI EELKKAGITSDYFDLINKAKTVEGVNALKDEILKAHA
BBL	1BAL	3	Yes	Yes	EEQNNDALSPAIRRLAEHNLDA SAIKGTGVGGRLTREDVEKHLAKA
Homeodomain	1DU0	1	Yes	Yes	RPRTAFSSEQLARLKRNFENRYLTERRRQQLSSELGLNEAQIKIWFANKRAKI
Homeodomain	1P7I	1	Yes	Yes	RPRTAFSSEQLARLKRNFENRYLTERRRQQLSSELGLNEAQIKIWFQARAKI
Homeodomain	1P7J	1	Yes	Yes	RPRTAFSSEQLARLKRNFENRYLTERRRQQLSSELGLNEAQIKIWFQNERAKI
Homeodomain	2HOS	4	Yes	Yes	RPRTAFSSEQLARLKRNFENRYLTERRRQQLSSELGLNEAQIKIWFKNMRAKI
Homeodomain	6M3D	2	Yes	Yes	RPRTAFSSEQLARLKRNFENRYLTERRRQQLSSELGLNEAQIKIWFKNKA AKI
Protein G	1GB1	10	No	No	MTYKL- - ILNGKTLKGETTTEAVDAATAEKVFKQYANDNGV DGEWYDDATKTFTVTE
Protein G	2GI9	11	No	No	MQYKL- - ILNGKTLKGETTTEAVDAATAEKVFKQYANDNGV DGEWYDDATKTFTVTE
Protein G	2J52	9	No	No	MTYKL- - ILNGKTLKGETTTEAVDAATAEKVFKQYANDNGV DGEWYDAATKTFTVTE
Protein G	5BMG	11	No	No	MQYKL- - ILNGKTLKGETTTEAVDAATAEKVFKQYANDNGV DGEWYDDATKTFTVTE
Protein G	1EM7	15	No	No	TTYKL- - ILNGKTLKGETTTEAVDAETAERVFKEYAKKNGV DGEWYDDATKTFTVTE
Protein G	1FCL	15	No	No	TTFKLI- - NGKTLKGETTTEAVDAATAEKVFKQYINDNGI DGEWYDDATKTFTVTE
Protein G	1MPE	16	No	No	MQYK- - VILNGKTLKGETTTEAVDAATFEKVVVKQFFNDNGV DGEWYDDATKTFTVTE
Protein G	1P7E	14	No	No	MQYKVI- - NGKTLKGETTTKAVDAETAEKAFKQYANDNGV DGVWYDDATKTFTVTE
Protein G	1Q10	15	No	No	MQYK- - VILNGKTLKGETTTEAVDAATAEKVVKQFFNDNGV DGEWYDDATKTFTVTE
Protein G	2KLL	12	No	No	MQYKL- - ILNGKTLKGETTTEAVDAATAEKVFKQYFNDNGV DGEWYDDATKTFTVTE
Protein G	2ON8	16	No	No	MQFKLI- - NGKTLKGETTTEAVDAEA EAEKFKQYANDNGI DGEWYDDATKTFTVTE
Protein G	2ONQ	16	No	No	MQFKLI- - NGKTLKGETTTEAVDAEA EAEKFKQYANDNGI DGEWYDDATKTFTVTE
Protein G	3V3X	13	No	No	MQYKLILCGKTLKGET- - TTEAVDAATAECVFKQYANDNGV DGEWYDDATKTFTVTE
Protein G	4WH4	14	No	No	MQYKLHLHGKTLKGET- - TTEAVDAATAEHVFKHYANDNGV DGEWYDDATKTFTVTE
Protein G	5BMH	12	No	No	MQYKL- - ILNGKTLKGETTTEAVDAATAEKVFKQYANDNGV DGEWCYDDATKTFTVTE
Protein G	5UB0	13	No	No	MTFKLI- - NGKTLKGETTTEAVDAATAEKVFKQYANDNGI DGEWYDDATKTFTVTE
Protein G	5UBS	14	No	No	MTFKLI- - NGKTLKGETTTEAVDAATAEKVFKQYFNDNGI DGEWYDDATKTFTVTE
Protein G	5UCE	14	No	No	MTFKAI- - NGKTLKGETTTEAVDAATAEKVFKQYFNDNGL DGEWYDDATKTFTVTE
Protein G	6NJF	13	No	No	MTFKLI- - NGKTLKGETTTEAVDAATAEKVFKQYANDNGL DGEWYDDATKTFTVTE
Protein G	6NL8	12	No	No	MTYKL- - ILNGKTHKGELTTEAVDAATAEKHFKQHANDLGV DGEWYDDATKTFTVTE
Protein G	6NLA	13	No	No	MTYKL- - ILNGKTHKGVLTIEAVDAATAEKHFKQHANDLGV DGEWYDDATKTFTVTE
Protein G	3FIL	12	No	No	MQYKL- - ILNGKTLKGVLTIEAVDAATAEKVFKQYANDLGV DGEWYDDATKTFTVTE
$\alpha$ 3D	2MTQ	3	Yes	Yes	MGSWAEFKQLAAIKTRCQALGGSEAECAAFEKE IAAFESLQAYKGGKNPEVEALRKEAAAIRDECQAYRHN
$\lambda$ -repressor	3KZ3	6	Yes	Yes	SLTQEQL EDARRLKA IWEKKKNEGLSYESVADKMGMGQS AVAALFNGINALNAYNAALLAKILKVSVEEFSPSIAREIR
$\lambda$ -repressor	1LLI	3	Yes	Yes	PLTQEQL EDARRLKA IYEKKKNEGLS QESLADKLGMGQS GIGALFNGINALNAYNAALLAKILKVSVEEFSPSIAREIY

## References

- (1) McCammon, J. Protein dynamics. *Reports on Progress in Physics* **1984**, *47*, 1.
- (2) Henzler-Wildman, K.; Kern, D. Dynamic personalities of proteins. *Nature* **2007**, *450*, 964–972.
- (3) Frauenfelder, H.; Sligar, S. G.; Wolynes, P. G. The energy landscapes and motions of proteins. *Science* **1991**, *254*, 1598–1603.
- (4) Diez, M.; Zimmermann, B.; Börsch, M.; König, M.; Schweinberger, E.; Steigmiller, S.; Reuter, R.; Felekyan, S.; Kudryavtsev, V.; Seidel, C. A., et al. Proton-powered subunit rotation in single membrane-bound F<sub>0</sub>F<sub>1</sub>-ATP synthase. *Nature structural & molecular biology* **2004**, *11*, 135–141.
- (5) Eisenmesser, E. Z.; Millet, O.; Labeikovsky, W.; Korzhnev, D. M.; Wolf-Watz, M.; Bosco, D. A.; Skalicky, J. J.; Kay, L. E.; Kern, D. Intrinsic dynamics of an enzyme underlies catalysis. *Nature* **2005**, *438*, 117–121.
- (6) McCammon, J. A.; Gelin, B. R.; Karplus, M. Dynamics of folded proteins. *Nature* **1977**, *267*, 585–590.
- (7) Karplus, M.; McCammon, J. A. Molecular dynamics simulations of biomolecules. *Nature structural biology* **2002**, *9*, 646–652.
- (8) Lindorff-Larsen, K.; Piana, S.; Dror, R. O.; Shaw, D. E. How fast-folding proteins fold. *Science (New York, N.Y.)* **2011**, *334*, 517–20.
- (9) Piana, S.; Lindorff-Larsen, K.; Shaw, D. E. Atomic-level description of ubiquitin folding. *Proceedings of the National Academy of Sciences* **2013**, *110*, 5915–5920.
- (10) Piana, S.; Lindorff-Larsen, K.; Shaw, D. E. Atomistic description of the folding of a dimeric protein. *The Journal of Physical Chemistry B* **2013**, *117*, 12935–12942.
- (11) Plattner, N.; Doerr, S.; De Fabritiis, G.; Noé, F. Complete protein–protein association kinetics in atomic detail revealed by molecular dynamics simulations and Markov modelling. *Nature chemistry* **2017**, *9*, 1005–1011.
- (12) Torrie, G. M.; Valleau, J. P. Nonphysical sampling distributions in Monte Carlo free-energy estimation: Umbrella sampling. *Journal of Computational Physics* **1977**, *23*, 187–199.
- (13) Frenkel, D.; Smit, B.; Ratner, M. A. *Understanding molecular simulation: from algorithms to applications*; Academic press San Diego, 1996; Vol. 2.
- (14) Sugita, Y.; Okamoto, Y. Replica-exchange molecular dynamics method for protein folding. *Chemical physics letters* **1999**, *314*, 141–151.
- (15) Fukunishi, H.; Watanabe, O.; Takada, S. On the Hamiltonian replica exchange method for efficient sampling of biomolecular systems: Application to protein structure prediction. *The Journal of chemical physics* **2002**, *116*, 9058–9067.
- (16) Izrailev, S.; Stepaniants, S.; Isralewitz, B.; Kosztin, D.; Lu, H.; Molnar, F.; Wriggers, W.; Schulten, K. *Computational molecular dynamics: challenges, methods, ideas*; Springer, 1999; pp 39–65.
- (17) Isralewitz, B.; Gao, M.; Schulten, K. Steered molecular dynamics and mechanical functions of proteins. *Current opinion in structural biology* **2001**, *11*, 224–230.

- (18) Laio, A.; Parrinello, M. Escaping free-energy minima. *Proceedings of the National Academy of Sciences* **2002**, *99*, 12562–12566.
- (19) Rezende, D.; Mohamed, S. Variational inference with normalizing flows. International conference on machine learning. 2015; pp 1530–1538.
- (20) Noé, F.; Olsson, S.; Köhler, J.; Wu, H. Boltzmann generators: Sampling equilibrium states of many-body systems with deep learning. *Science* **2019**, *365*.
- (21) Chavez, L. L.; Onuchic, J. N.; Clementi, C. Quantifying the roughness on the free energy landscape: entropic bottlenecks and protein folding rates. *Journal of the American Chemical Society* **2004**, *126*, 8426–8432.
- (22) Das, P.; Matysiak, S.; Clementi, C. Balancing energy and entropy: A minimalist model for the characterization of protein folding landscapes. *Proceedings of the National Academy of Sciences* **2005**, *102*, 10141–10146.
- (23) Levitt, M.; Warshel, A. Computer simulation of protein folding. *Nature* **1975**, *253*, 694–698.
- (24) Marrink, S. J.; Tieleman, D. P. Perspective on the Martini model. *Chemical Society Reviews* **2013**, *42*, 6801–6822.
- (25) Machado, M. R.; Barrera, E. E.; Klein, F.; Sónora, M.; Silva, S.; Pantano, S. The SIRAH 2.0 force field: altius, fortius, citius. *Journal of chemical theory and computation* **2019**, *15*, 2719–2733.
- (26) Saunders, M. G.; Voth, G. A. Coarse-graining methods for computational biology. *Annual review of biophysics* **2013**, *42*, 73–93.
- (27) Izvekov, S.; Voth, G. A. A multiscale coarse-graining method for biomolecular systems. *The Journal of Physical Chemistry B* **2005**, *109*, 2469–2473.
- (28) Noid, W. G. Perspective: Coarse-grained models for biomolecular systems. *The Journal of chemical physics* **2013**, *139*, 09B201\_1.
- (29) Clementi, C. Coarse-grained models of protein folding: toy models or predictive tools? *Current opinion in structural biology* **2008**, *18*, 10–15.
- (30) Clementi, C.; Nymeyer, H.; Onuchic, J. N. Topological and energetic factors: what determines the structural details of the transition state ensemble and “en-route” intermediates for protein folding? An investigation for small globular proteins. *Journal of molecular biology* **2000**, *298*, 937–953.
- (31) Marrink, S. J.; Risselada, H. J.; Yefimov, S.; Tieleman, D. P.; De Vries, A. H. The MARTINI force field: coarse grained model for biomolecular simulations. *The journal of physical chemistry B* **2007**, *111*, 7812–7824.
- (32) Monticelli, L.; Kandasamy, S. K.; Periole, X.; Larson, R. G.; Tieleman, D. P.; Marrink, S.-J. The MARTINI coarse-grained force field: extension to proteins. *Journal of chemical theory and computation* **2008**, *4*, 819–834.
- (33) Koliński, A., et al. Protein modeling and structure prediction with a reduced representation. *Acta Biochimica Polonica* **2004**, *51*.
- (34) Davtyan, A.; Schafer, N. P.; Zheng, W.; Clementi, C.; Wolynes, P. G.; Papoian, G. A. AWSEM-MD: protein structure prediction using coarse-grained physical potentials and bioinformatically based local structure biasing. *The Journal of Physical Chemistry B* **2012**, *116*, 8494–8503.

- (35) Das, R.; Baker, D. Macromolecular modeling with rosetta. *Annual review of biochemistry* **2008**, *77*, 363–382.
- (36) Wang, W.; Gómez-Bombarelli, R. Coarse-graining auto-encoders for molecular dynamics. *npj Computational Materials* **2019**, *5*, 1–9.
- (37) Boninsegna, L.; Banisch, R.; Clementi, C. A data-driven perspective on the hierarchical assembly of molecular structures. *Journal of Chemical Theory and Computation* **2018**, *14*, 453–460.
- (38) Foley, T. T.; Shell, M. S.; Noid, W. G. The impact of resolution upon entropy and information in coarse-grained models. *The Journal of chemical physics* **2015**, *143*, 12B601\_1.
- (39) Foley, T. T.; Kidder, K. M.; Shell, M. S.; Noid, W. Exploring the landscape of model representations. *Proceedings of the National Academy of Sciences* **2020**, *117*, 24061–24068.
- (40) Ruza, J.; Wang, W.; Schwalbe-Koda, D.; Axelrod, S.; Harris, W. H.; Gómez-Bombarelli, R. Temperature-transferable coarse-graining of ionic liquids with dual graph convolutional neural networks. *The Journal of Chemical Physics* **2020**, *153*, 164501.
- (41) Duvenaud, D.; Maclaurin, D.; Aguilera-Iparraguirre, J.; Gómez-Bombarelli, R.; Hirzel, T.; Aspuru-Guzik, A.; Adams, R. P. Convolutional networks on graphs for learning molecular fingerprints. *arXiv preprint arXiv:1509.09292* **2015**,
- (42) Husic, B. E.; Charron, N. E.; Lemm, D.; Wang, J.; Pérez, A.; Majewski, M.; Krämer, A.; Chen, Y.; Olsson, S.; de Fabritiis, G., et al. Coarse graining molecular dynamics with graph neural networks. *The Journal of Chemical Physics* **2020**, *153*, 194101.
- (43) Wang, J.; Olsson, S.; Wehmeyer, C.; Pérez, A.; Charron, N. E.; De Fabritiis, G.; Noé, F.; Clementi, C. Machine learning of coarse-grained molecular dynamics force fields. *ACS central science* **2019**, *5*, 755–767.
- (44) Nüske, F.; Boninsegna, L.; Clementi, C. Coarse-graining molecular systems by spectral matching. *The Journal of chemical physics* **2019**, *151*, 044116.
- (45) Wang, J.; Chmiela, S.; Müller, K.-R.; Noé, F.; Clementi, C. Ensemble learning of coarse-grained molecular dynamics force fields with a kernel approach. *The Journal of Chemical Physics* **2020**, *152*, 194106.
- (46) Zhang, L.; Han, J.; Wang, H.; Car, R.; E, W. DeePCG: Constructing coarse-grained models via deep neural networks. *The Journal of chemical physics* **2018**, *149*, 034101.
- (47) Chen, Y.; Krämer, A.; Charron, N. E.; Husic, B. E.; Clementi, C.; Noé, F. Machine learning implicit solvation for molecular dynamics. *The Journal of Chemical Physics* **2021**, *155*, 084101.
- (48) Unke, O. T.; Chmiela, S.; Gastegger, M.; Schütt, K. T.; Sauceda, H. E.; Müller, K.-R. SpookyNet: Learning force fields with electronic degrees of freedom and nonlocal effects. *Nature communications* **2021**, *12*, 1–14.
- (49) Unke, O. T.; Stöhr, M.; Ganscha, S.; Unterthiner, T.; Maennel, H.; Kashubin, S.; Ahlin, D.; Gastegger, M.; Sandonas, L. M.; Tkatchenko, A., et al. Accurate Machine Learned Quantum-Mechanical Force Fields for Biomolecular Simulations. *arXiv preprint arXiv:2205.08306* **2022**,
- (50) Unke, O. T.; Meuwly, M. PhysNet: A neural network for predicting energies, forces, dipole moments, and partial charges. *Journal of chemical theory and computation* **2019**, *15*, 3678–3693.



- (51) Wang, J.; Charron, N.; Husic, B.; Olsson, S.; Noé, F.; Clementi, C. Multi-body effects in a coarse-grained protein force field. *The Journal of Chemical Physics* **2021**, *154*, 164113.
- (52) Behler, J.; Parrinello, M. Generalized neural-network representation of high-dimensional potential-energy surfaces. *Physical review letters* **2007**, *98*, 146401.
- (53) Rupp, M.; Tkatchenko, A.; Müller, K.-R.; Von Lilienfeld, O. A. Fast and accurate modeling of molecular atomization energies with machine learning. *Physical review letters* **2012**, *108*, 058301.
- (54) Smith, J. S.; Isayev, O.; Roitberg, A. E. ANI-1: an extensible neural network potential with DFT accuracy at force field computational cost. *Chemical science* **2017**, *8*, 3192–3203.
- (55) Schütt, K. T.; Sauceda, H. E.; Kindermans, P.-J.; Tkatchenko, A.; Müller, K.-R. SchNet—a deep learning architecture for molecules and materials. *The Journal of Chemical Physics* **2018**, *148*, 241722.
- (56) Unke, O. T.; Meuwly, M. PhysNet: A Neural Network for Predicting Energies, Forces, Dipole Moments and Partial Charges. *arXiv:1902.08408 [physics]* **2019**, arXiv: 1902.08408.
- (57) Qiao, Z.; Welborn, M.; Anandkumar, A.; Manby, F. R.; Miller III, T. F. OrbNet: Deep Learning for Quantum Chemistry Using Symmetry-Adapted Atomic-Orbital Features. *arXiv:2007.08026 [physics]* **2020**, arXiv: 2007.08026.
- (58) Kubelka, J.; Hofrichter, J.; Eaton, W. A. The protein folding ‘speed limit’. *Current opinion in structural biology* **2004**, *14*, 76–88.
- (59) Shell, M. S. The relative entropy is fundamental to multiscale and inverse thermodynamic problems. *The Journal of chemical physics* **2008**, *129*, 144108.
- (60) Noid, W. G.; Chu, J.-W.; Ayton, G. S.; Krishna, V.; Izvekov, S.; Voth, G. A.; Das, A.; Andersen, H. C. The multiscale coarse-graining method. I. A rigorous bridge between atomistic and coarse-grained models. *The Journal of chemical physics* **2008**, *128*, 244114.
- (61) Thaler, S.; Zavadlav, J. Learning neural network potentials from experimental data via Differentiable Trajectory Reweighting. *Nature communications* **2021**, *12*, 1–10.
- (62) Doerr, S.; Majewski, M.; Pérez, A.; Krämer, A.; Clementi, C.; Noe, F.; Giorgino, T.; De Fabritiis, G. TorchMD: A deep learning framework for molecular simulations. *Journal of chemical theory and computation* **2021**, *17*, 2355–2363.
- (63) Husic, B. E.; Pande, V. S. Markov state models: From an art to a science. *Journal of the American Chemical Society* **2018**, *140*, 2386–2396.
- (64) Prinz, J. H.; Wu, H.; Sarich, M.; Keller, B.; Senne, M.; Held, M.; Chodera, J. D.; Schütte, C.; Noé, F. Markov models of molecular kinetics: Generation and validation. *Journal of Chemical Physics* **2011**, *134*.
- (65) Singhal, N.; Snow, C. D.; Pande, V. S. Using path sampling to build better Markovian state models: Predicting the folding rate and mechanism of a tryptophan zipper beta hairpin. *J. Chem. Phys.* **2004**, *121*, 415–425.
- (66) Noé, F.; Fischer, S. Transition networks for modeling the kinetics of conformational change in macromolecules. *Current Opinion in Structural Biology* **2008**, *18*, 154–162.
- (67) Pan, A. C.; Roux, B. Building Markov state models along pathways to determine free energies and rates of transitions. *J. Chem. Phys.* **2008**, *129*.

- (68) Zemla, A. LGA: a method for finding 3D similarities in protein structures. *Nucleic acids research* **2003**, *31*, 3370–3374.
- (69) Pérez-Hernández, G.; Paul, F.; Giorgino, T.; De Fabritiis, G.; Noé, F. Identification of slow molecular order parameters for Markov model construction. *The Journal of chemical physics* **2013**, *139*, 07B604\_1.
- (70) Schwantes, C. R.; Pande, V. S. Improvements in Markov State Model construction reveal many non-native interactions in the folding of NTL9. *J. Chem. Theory Comput.* **2013**, *9*, 2000–2009.
- (71) McCallister, E. L.; Alm, E.; Baker, D. Critical role of  $\beta$ -hairpin formation in protein G folding. *Nature structural biology* **2000**, *7*, 669–673.
- (72) Kmiecik, S.; Kolinski, A. Folding pathway of the B1 domain of protein G explored by multiscale modeling. *Biophysical journal* **2008**, *94*, 726–736.
- (73) Kuhlman, B.; Baker, D. Exploring folding free energy landscapes using computational protein design. *Current opinion in structural biology* **2004**, *14*, 89–95.
- (74) Jumper, J.; Evans, R.; Pritzel, A.; Green, T.; Figurnov, M.; Ronneberger, O.; Tunyasuvunakool, K.; Bates, R.; Žídek, A.; Potapenko, A.; Bridgland, A.; Meyer, C.; Kohl, S. A. A.; Ballard, A. J.; Cowie, A.; Romera-Paredes, B.; Nikolov, S.; Jain, R.; Adler, J.; Back, T.; Petersen, S.; Reiman, D.; Clancy, E.; Zielinski, M.; Steinegger, M.; Pacholska, M.; Berghammer, T.; Bodenstein, S.; Silver, D.; Vinyals, O.; Senior, A. W.; Kavukcuoglu, K.; Kohli, P.; Hassabis, D. Highly accurate protein structure prediction with AlphaFold. *Nature* **2021**,
- (75) Baek, M.; DiMaio, F.; Anishchenko, I.; Dauparas, J.; Ovchinnikov, S.; Lee, G. R.; Wang, J.; Cong, Q.; Kinch, L. N.; Schaeffer, R. D., et al. Accurate prediction of protein structures and interactions using a three-track neural network. *Science* **2021**, *373*, 871–876.
- (76) Thölke, P.; De Fabritiis, G. TorchMD-NET: Equivariant Transformers for Neural Network based Molecular Potentials. *arXiv preprint arXiv:2202.02541* **2022**,
- (77) Harvey, M. J.; Giupponi, G.; De Fabritiis, G. ACEMD: Accelerating biomolecular dynamics in the microsecond time scale. *Journal of Chemical Theory and Computation* **2009**, *5*, 1632–1639.
- (78) Buch, I.; Harvey, M. J.; Giorgino, T.; Anderson, D. P.; De Fabritiis, G. High-throughput all-atom molecular dynamics simulations using distributed computing. *J. Chem. Inf. Model.* **2010**, *50*, 397–403.
- (79) Piana, S.; Lindorff-Larsen, K.; Shaw, D. E. How robust are protein folding simulations with respect to force field parameterization? *Biophysical Journal* **2011**, *100*.
- (80) Jorgensen, W. L.; Chandrasekhar, J.; Madura, J. D.; Impey, R. W.; Klein, M. L. Comparison of simple potential functions for simulating liquid water. *J. Chem. Phys.* **1983**, *79*, 926–935.
- (81) Doerr, S.; De Fabritiis, G. On-the-Fly Learning and Sampling of Ligand Binding by High-Throughput Molecular Simulations. *Journal of Chemical Theory and Computation* **2014**,
- (82) Feenstra, K. A.; Hess, B.; Berendsen, H. J. Improving efficiency of large time-scale molecular dynamics simulations of hydrogen-rich systems. *J. Comput. Chem.* **1999**, *20*, 786–798.

- (83) Pérez, A.; Herrera-Nieto, P.; Doerr, S.; De Fabritiis, G. AdaptiveBandit: A multi-armed bandit framework for adaptive sampling in molecular simulations. *Journal of Chemical Theory and Computation* **2020**, *16*, 4685–4693.
- (84) Doerr, S.; Harvey, M. J.; Noé, F.; De Fabritiis, G. HTMD: High-Throughput Molecular Dynamics for Molecular Discovery. *Journal of Chemical Theory and Computation* **2016**, *12*, 1845–1852.
- (85) Paszke, A.; Gross, S.; Massa, F.; Lerer, A.; Bradbury, J.; Chanan, G.; Killeen, T.; Lin, Z.; Gimelshein, N.; Antiga, L., et al. Pytorch: An imperative style, high-performance deep learning library. *Advances in neural information processing systems* **2019**, *32*, 8026–8037.
- (86) Schutt, K.; Kessel, P.; Gastegger, M.; Nicoli, K.; Tkatchenko, A.; Müller, K.-R. SchNetPack: A deep learning toolbox for atomistic systems. *Journal of chemical theory and computation* **2018**, *15*, 448–455.
- (87) Fey, M.; Lenssen, J. E. Fast graph representation learning with PyTorch Geometric. *arXiv preprint arXiv:1903.02428* **2019**,
- (88) Falcon, e. a., WA PyTorch Lightning. 2019.
- (89) Schrödinger, LLC, The PyMOL Molecular Graphics System, Version 2.5.0, Schrödinger, LLC. <https://github.com/schrodinger/pymol-open-source>, 2022.